The spectrum of the Elastic Rayleigh Equation

A Thesis
Submitted for the Degree of
MASTER OF SCIENCE (ENGINEERING)

by

J. SHASHI KIRAN REDDY

ENGINEERING MECHANICS UNIT
JAWAHARLAL NEHRU CENTRE FOR ADVANCED SCIENTIFIC RESEARCH
(A Deemed University)
Bangalore – 560 064

OCTOBER 2015

Mother Nature and My Parents.....

DECLARATION

I hereby declare that the matter embodied in the thesis entitled "**The spectrum of the Elastic Rayleigh Equation**" is the result of investigations carried out by me at the Engineering Mechanics Unit, Jawaharlal Nehru Centre for Advanced Scientific Research, Bangalore, India under the supervision of **Dr. Ganesh Subramanian** and that it has not been submitted elsewhere for the award of any degree or diploma.

In keeping with the general practice in reporting scientific observations, due acknowledgment has been made whenever the work described is based on the findings of other investigators.

J. Shashi Kiran Reddy

CERTIFICATE

I hereby certify that the matter embodied in this thesis entitled "**The spectrum of the Elastic Rayleigh Equation**" has been carried out by **Mr. J. Shashi Kiran Reddy** at the Engineering Mechanics Unit, Jawaharlal Nehru Centre for Advanced Scientific Research, Bangalore, India under my supervision and that it has not been submitted elsewhere for the award of any degree or diploma.

Dr. Ganesh Subramanian
(Research Supervisor)

Acknowledgements

I feel it is my sincere duty to acknowledge the people who have directly or indirectly helped me during my stay in JNC intellectually or otherwise. First and foremost, I would like to express my sincere gratitude to my supervisor, *Dr. Ganesh Subramanian*, who right from the beginning of my research provided me all the facilities he could offer to carry out my research and monitored my work. His guidance added with support and encouragement that he has provided during the course of the work, and the immense patience that he has invested in me have been a constant source of inspiration.

I would like to thank *Prof. K.R.Sreenivas* for his support and encouragement throughout my stay and also for his course work. I shall ever be thankful to *Prof. Maheboob Alam* for his valuable courses.

I am extremely thankful to present and past members of the lab−*Navaneeth, Anubhab, Sankalp*, *Vicky, Arun, Praveen, Prasanth, Ponnu, Rajesh, Rafi, Achal, Saikath, Saikishan* and others for providing a stimulating and fun environment in which to learn and grow. I am greatly thankful to my B.Tech Professor *A.K.Verma*, for his inspiring life and wonderful courses. I owe loving thanks to my wonderful friends from B.Tech days; *Vijay, Yeshwanth, vipul, Ishan, Abhi Mitra*, *Sampath* and *Narender* for being part of this journey, spreading good cheer and constantly encouraging me to get through the difficult times. My heartfelt thanks to *Susheela*, for she is the one who listens to my crazy ideas about life, medicinal plants, astrobiology and other things patiently. I am very grateful to *Swathi, Manoj* and *Bhawani* for their love, affection and care.

I thank JNC administrative officer, Mr. A.N.*Jayachandra*, other *admin*, *library*, *complab* and *gardening* staff, for various helps from time to time. My special thanks to JNC garden supervisor, *Jayaramayya*, for his beautiful garden and also for sharing his knowledge on medicinal plants. Finally let me thank JNCASR and DST for providing all the financial and infrastructural support and I am sincerely grateful for that.

I would like to take this special opportunity to thank my parents and loving sister who have been very supportive despite of all the difficulties. My special thanks to *Dominic Baba* for his special relationship and also for cheering me up with his mystical experiences. Above all, I would like to thank the almighty God, for it is under his grace that we live, learn and flourish and I dedicate this work to *Mother Nature.*

Abstract

Fluids have fascinated many generations of scientists and engineers. Although a considerable amount of research has been devoted to the study of fluids of low molecular weight (well described by the Navier-Stokes equations), many challenging problems in both theory and applications still remain. But, even more challenging are non-Newtonian fluids, whose motions cannot be described by the Navier-Stokes equations. The present work would be of fundamental importance to the dynamics of fast flows of a class of such fluids (dilute polymeric solutions). Here, we consider a well-known theoretical model (Oldroyd-B fluid) in order to represent, in the simplest possible manner, the polymer-solvent coupling in a dilute polymer solution, and study how the resulting non-Newtonian rheology affects the known structure of the continuous spectrum in the inviscid limit. In general, the equation governing the evolution of small-amplitude perturbations to inviscid shearing flows, the Rayleigh equation, is singular, and the continuous spectra associated with the Rayleigh equation owe their origin to such singular points. Additional continuous spectra exist with the introduction of elasticity, and it has already been shown, in the inertialess limit, that the nature of the continuous spectrum is sensitive to the base-state velocity profile and the particular constitutive model used (UCM v/s Oldroyd-B; Wilson *et al.* (1999)). The viscoelastic continuous spectra owe their origin to the 'simple fluid' assumption underlying almost all constitutive equations used in polymer rheology. The fact that the polymeric stress only depends on the evolution of the polymer conformation along a particular streamline, and is not influenced by the polymer molecules convected by streamlines in the immediate vicinity, supports the existence of continuous spectra in elastic liquids, and this is independent of the Reynolds number. In this thesis, we study the nature of the elastic continuous spectrum at large Reynolds number which serves as a complement to the aforementioned study of Wilson *et al.* (1999) in the absence of inertia.

The initial part of the thesis is mainly concerned with the study of the nature of the continuous spectrum of the so-called elastic Rayleigh equation (ERE), one that governs the small amplitude perturbations in the limit of the Reynolds (Re) and the Deborah (De) numbers approaching infinity, with E, the elastic number, defined as $(1-\beta)De/Re$, where ’β’ is the ratio of the solvent viscosity to total viscosity)) being finite. We analyze the problem within the framework of linear stability theory, for two canonical flows: Couette flow and the Rankine vortex, for which the purely inviscid spectra have been completely characterized. These serve as useful starting points for the general analysis of the dynamics of two-dimensional perturbations in an arbitrary plane parallel shearing flow. It is shown that in addition to the continuous spectrum of the familiar inviscid Rayleigh equation, one that spans the base-state range of velocities (Case (1960); Drazin & Reid (1981)), the elastic Rayleigh equation exhibits a pair of continuous spectra that may be associated with neutrally stable slow and fast elastic shear waves (travelling waves) propagating with (non-dimensional) speeds proportional to $\pm\sqrt{2E}$ relative to the local flow (the neglect of the relaxation terms in the limit ($De \to \infty$) implies that the polymer solution supports undamped elastic shear waves). The existence of these shear waves leads to multiple (three) continuous spectra associated with the elastic Rayleigh equation in contrast to just one for the original Rayleigh equation. The final part of the thesis discusses the additional effects of relaxation terms (De being finite but large). In this case only the continuous spectrum associated with the critical-level survives, and the ones associated with the aforementioned travelling waves are no longer preserved.

List of Figures

1.1 Non-Newtonian fluid properties . . . 3

2.1 Distribution of different regions in Couette flow . . . 16
2.2 Matching in Couette flow . . . 17
2.3 Elastic Couette flow spectrum with 'E(=0.01)' fixed .(a) N=300 (b) N=450 (c) N=600 (d) N=1200 . . . 24
2.4 Elastic Couette flow spectrum with 'N (=600)' fixed. (a) E=0.01 (b) E=0.1 (c) E=0.5 (d) E=0.7 . . . 25
2.5 Eigenfunctions over complete spectrum.(a) An $FSWS$ eigenfunction (b) A superposition of the $FSWS$ and the Doppler eigenfunctions (c) A superposition of the $FSWS$, Doppler, and the $SSWS$ eigenfunctions (d) A superposition of the $SSWS$ and the Doppler eigenfunctions (e) An $SSWS$ eigenfunction . . . 26

3.1 Distribution of different regions in elastic vortex . . . 40
3.2 Matching inner and outer regions . . . 42

4.1 Finite De scheme . . . 57

Contents

Abstract vii

List of Figures ix

1 Introduction 1

1.1 Introduction 1

1.2 Importance of the Continuous spectrum 2

1.3 Theory of Non-Newtonian fluids 4

1.3.1 Constitutive equations 5

1.4 Organization of the thesis 6

2 Elastic Coeutte flow 7

2.1 Introduction 7

2.2 Problem formulation 9

2.2.1 The continuous spectrum for finite Re and De 11

2.3 Elastic Rayleigh equation (Re→ ∞ and De→ ∞) 12

2.4 Boundary layer analysis of the (elastic Rayleigh equation) for small but finite E . 14

2.4.1 The outer solutions 14

2.4.2 Matching the inner (boundary layer) and the outer solutions 17

2.4.3 Perturbation vorticity field 18

2.4.4 Uniformly valid analysis 20

2.5 Numerical results 23

3 Elastic Rankine Vortex 29

3.1 Introduction 29

3.2 Problem formulation 30

3.2.1 The Continuous spectrum for finite Re and De 31
3.3 Elastic Rayleigh Equation (Re→ ∞ and De→ ∞) 33
3.4 Boundary layer analysis of the elastic Rayleigh equation 35
3.4.1 The outer solutions 36
3.4.2 Matching the inner (boundary layer) and outer solutions: 41
3.4.3 Perturbation vorticity field 45
3.4.4 Uniformly valid analysis 49
3.5 Conclusion 50

4 Finite De analysis **53**

4.1 Introduction 53
4.1.1 Boundary layer analysis at the critical level 55
4.1.2 Boundary layer analysis at travelling waves locations 56
4.1.3 Matching at the travelling-wave singularities 58

5 Conclusions and Future Work **63**

References **65**

Chapter 1

Introduction

1.1 Introduction

The flows of non-Newtonian/complex fluids, which are ubiquitous in our everyday life, fascinate not only fluid dynamicists with their complexity, but also playful kids with their peculiarity. The complex behavior of non-Newtonian fluids originates from the strong interaction between the external flow and the internal micro-structure of the fluid. For example, if we consider water (a Newtonian fluid), the motion of water molecules is largely unaffected by the external flow on account of the immensely disparate time scales involved, while in flows of viscoelastic liquids, the slowly relaxing micro-structure gets significantly stretched and deformed, where the relaxation time depends on the solvent viscosity and polymer molecular weight. Since these interactions are partly reversible and depend on the deformation history, the fluid acquires memory and becomes elastic. The presence of elasticity has several striking consequences including rod climbing, die swell and the tubeless siphon effect etc (Bird *et al.* (1987); Macosko (1994)). Understanding polymer fluid dynamics is important in connection with plastics manufacture, performance of lubricants, application of paints, processing of foodstuffs, and movement of biological fluids. The study of polymeric flows has already attracted great attention towards the end of the last century owing to the discovery of purely elastic instabilities that owe their origin solely due to elasticity, and can, in sharp contrast to Newtonian fluids, arise even in the absence of inertia. As a result, these flows can transition to disorderly flows even at very small Reynolds numbers, a state referred to as elastic turbulence (Larson *et al.* (1990); Groisman & V.Steinberg (2000)). The aforementioned complexity of the observed dynamical phenomena is reflected in the governing equations for complex fluids, where the equations of motion are supplemented by a non-trivial constitutive equation in a differential or integral form.

While the aforementioned elastic turbulence is primarily of relevance to slow flows of complex fluids, the present study would be of fundamental importance to the dynamics of fast flows of these non-Newtonian liquids (polymer solutions in particular). For simplicity we restrict our present study to the stability of dilute polymeric solutions. The stability investigations for viscoelastic flows started with the pioneering work of Gorodtsov & Leonov (1967) in the context of plain Couette flow, followed by various studies neglecting inertia (Renardy (1992); Kupferman (2005); Wilson *et al.* (1999)) for other plane-parallel flows. The combined effects of inertia and viscoelasticity on flow instabilities have been studied extensively only for a few classes of simple parallel flows, specifically plane Couette and Poiseuille flows (Porteous & M.M.Denn (1972)), the hyperbolic-tangent shear layer (Azaiez & Homsy (1994); Kaffel & Renardy (2010)) and the submerged elastic jet (Rallison & Hinch (1995)). The results show that although the elasticity in general has a stabilizing effect on the purely inviscid instabilities (Kaffel & Renardy (2010)), this is not always the case, and there are examples where a small amount of elasticity actually destabilizes the flow (Rallison & Hinch (1995)). While inertialess stability investigatiomns have focussed on the nature of the viscoelastic continuous spectra, those that include inertia (at high Reynolds numbers) have focussed solely on the discrete modes. The thesis helps partially fill this void by examining the nature of the elastic continuous spectra at high Reynolds numbers. In light of the known analogy between the governing equations for a polymer solution in the relaxationless limit (Ogilvie & Proctor (2003); Roy (2012)), and those that result for magnetohydrodynamic (MHD) flows at high magnetic Reynolds numbers, the contents of this thesis may also be relevant to the MHD context.

We commence this introductory chapter with a discussion on the importance of the continuous spectrum modes in section (1.2). Section (1.3) comments on the peculiar behavior of non-Newtonian fluids in comparison to those of Newtonian fluids, and briefly overviews some commonly used constitutive models. Section (1.4) provides an outline for the remainder of the thesis.

1.2 Importance of the Continuous spectrum

"The question of determining if a general solution can be expressed as an infinite sum of such solutions is the completeness problem, which is in general difficult." -Saffman [1992] .

In the context of linear stability (modal) analysis, the eigenspectrum of the equation governing infinitesimal perturbations consists of a discrete part containing separated eigenvalues (the eigenfunctions being referred to as the discrete modes) and one or more continuous intervals

Time dependence: Relaxing modulus	**Normal stress in shear (>0):** Weissenberg effect
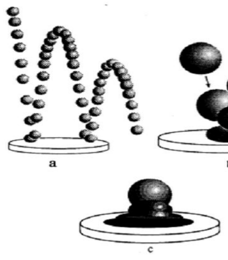	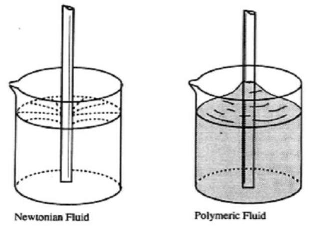
Simplest example that shows this dependence is the common toy **'Silly Putty'** or **'bouncing putty.'** When a stress acts on silly putty for only a short time (a, b), the material behaves like a solid, bouncing back when dropped; but when stressed for several hours (c), it flows out like a liquid .	A rod is rotated in a beaker of motor oil on the left and in a solution of 1% polyisobutylene in oil on the right. When a rod is rotated in a beaker of Newtonian liquid (water, oil etc), inertial forces cause it to move away from rod, but for polymer solution, it will climb the rod.

(a)

Extensional thickening viscosity	**Shear thinning (or thickening) viscosity**
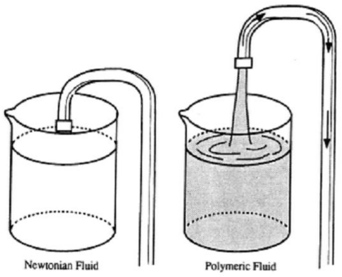	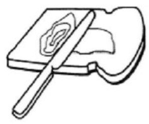
The 'ductless siphon,' shows this property. When a siphon is slowly removed from a Newtonian fluid, it breaks very close to the surface, but some complex fluids can be pulled up many centimeters above the free surface.	If a mayonnaise is left on a piece of bread subject only to stresses due to gravity, it will barely move, but when sheared by a knife it spreads easily. In contrast, honey, which is more viscous than mayonnaise at high stresses, will slowly run through holes in the bread. The viscosity of honey is constant, but the viscosity of mayonnaise depends strongly on the shear stress.

(b)

Figure 1.1: Non-Newtonian fluid properties

(corresponding to the continuous spectrum modes). In the classical regular Sturm- Liouville framework, the spectrum is entirely discrete, and consists of a denumerable infinity of eigenfunctions that form a complete basis. However, in eigenvalue problems typically associated with inviscid shearing flows, the discrete part of the spectrum may only contain a finite number of eigenvalues or no eigenvalues at all (as is the case with inviscid Couette flow; (Case (1960); Drazin & Reid (1981)), and thereby, is evidently incomplete. For instance, the spectrum of the governing Rayleigh equation is purely continuous for any non-inflectional base-state velocity profile (inviscid Couette flow above being a special case). In general, if we assume the normal modes to form a complete basis, we should be able to express an arbitrary disturbance as a summation over the discrete spectrum eigenfunctions together with an integral over the continuous spectrum eigenfunctions, both contributions being weighted by appropriate complex-valued amplitudes. The continuous spectrum can arise as a result of solving the problem on an infinite domain (Friedman (1962)). Of more relevance to inviscid stability problems is the case where the continuous spectrum arises due to the governing differential equation containing coefficients that become singular at points within the domain (Drazin & Reid (1981)). An important feature of the eigenfunctions that compose the resulting continuous spectrum is that they are not regular functions; typically, they are characterized by irregular shapes, and require a generalized function interpretation (Engevik (1971); Balmforth & Morrison (1995*a*)). The present work comes under the framework of hydrodynamic stability and aims to study as to how the inviscid continuous spectrum would be modified with the addition of elasticity.

1.3 Theory of Non-Newtonian fluids

"While it is true that the classical definition of liquid as opposed to solid provides a basis for deciding whether a substance is a solid or a liquid, the classical definition is inadequate not only for many everyday purposes , but for engineering ones as well." -Ronald G. Larson

In this section we comment on some important properties of these fluids - the ones that make them different from the commonly observed Newtonian fluids - with day-to-day examples; see figure (1.1). Numerous experiments illustrate the four most important phenomena in their rheology (Macosko (1994)).

1.3.1 Constitutive equations

1.3.1.1 The upper convected derivative

The fluids we study (polymer solutions) have a viscoelastic character. Thus, besides the usual viscous response (already present for Newtonian fluids), one needs the notion of an elastic strain which depends on the history of rotation and stretching in the flow. The constitutive equations used possess this information. This is accomplished by the upper convected derivative of a tensor '$\mathbf{X}$' denoted by '$\overset{\triangledown}{\mathbf{X}}$' and defined as:

$$\overset{\triangledown}{\mathbf{X}} \equiv \frac{D\mathbf{X}}{Dt} - (\nabla \mathbf{v})^{\dagger}.\mathbf{X} - \mathbf{X}.(\nabla \mathbf{v}). \tag{1.1}$$

where D/Dt is the usual material derivative. This derivative contains not only the advection associated with the material derivative, but also accounts for rotation and stretching with the flow like a material element through the terms involving $\nabla \mathbf{v}$ and $\nabla \mathbf{v}^{\dagger}$; that is, the derivative is co-deformational in character (Bird *et al.* (1987)). It can also be interpreted as a frame-invariant derivative which describes the frozen state of a second order tensor field ($\mathbf{X}$) in a velocity field $\mathbf{v}$.

1.3.1.2 Oldroyd-B fluid

One of the simplest constitutive equations, that serves as a theoretical model for so-called Boger fluids (see below), and that uses the upper convected derivative above, is the Oldroyd-B model. From a microscopic point of view, the Oldroyd-B constitutive relation results from modeling dilute polymer solution as a non-interacting suspension of infinitely extensible Hookean dumbbells (Larson (1988)). The Oldroyd-B constitutive relation is given by:

$$\boldsymbol{\sigma}_d + \lambda_1 \overset{\triangledown}{\boldsymbol{\sigma}}_d = 2\mu(\mathbf{E} + \lambda_2 \overset{\triangledown}{\mathbf{E}}), \tag{1.2}$$

where $\boldsymbol{\sigma}_d$ is the deviatoric stress, μ is the total viscosity, λ_1 the relaxation time and λ_2 the retardation time. Here, $\lambda_2 \to \lambda_1$ denotes the Newtonian limit, while $\lambda_2 = 0$ corresponds to the upper-convected Maxwell (UCM) fluid, a simple model for a polymer melt. '$\triangledown$' in (1.2) denotes the upper-convected derivative defined above in section (1.3.1). On writing the total stress as the sum of a solvent and a polymer contribution of the form $\boldsymbol{\sigma}_d = 2\mu^*\mathbf{E} + G\mathbf{A}$ with $\mathbf{A}$ being the non-dimensional conformation tensor ($\mathbf{A} \propto \mathbf{RR}$), $\mu^* = \mu\lambda_2/\lambda_1$ (the solvent viscosity), $\mu_p = \mu - \mu^*$ (the polymer viscosity) and $G = \mu_p/\lambda_1$ (the shear modulus), we have the following set of governing equations for the motion of an Oldroyd-B fluid (Roy (2012)):

$$\begin{aligned} \rho\frac{D\mathbf{v}}{Dt} &= -\nabla p^* + \mu^*\nabla^2\mathbf{v} + G\nabla.\mathbf{A}, && (1.3)\\ \overset{\triangledown}{\mathbf{A}} &= -\frac{1}{\tau}(\mathbf{A}-\mathbf{I}), && (1.4)\\ \nabla.\mathbf{v} &= 0, && (1.5) \end{aligned}$$

where $\tau = \lambda_1$ and $p^* = p + 2(1 - \lambda_2/\lambda_1)\mu/\lambda_1$.

1.3.1.3 The Boger fluid

An Oldroyd-B fluid is an example of an ideal elastic fluid which exhibits a constant viscosity and constant normal stress coefficients in simple shear flow. Boger (1977) developed a class of fluids whose experimental measurements shown to have effectively constant viscosity and normal stress coefficients over a range of shear rates.

1.4 Organization of the thesis

In the present work, we analyze within the framework of linear stability theory, for two canonical inviscid flows of a dilute polymer solution - Couette flow and the Rankine vortex. These serve as useful starting points for the general analysis of the dynamics of two-dimensional perturbations in an elastic shearing flow. In chapter [2], we study the effects of elasticity, on the known structure of the continuous spectrum eigenfunctions, in the inviscid limit (Re $\rightarrow \infty$) for Couette flow. Here, we look at the regime characterized by high values of De and Re with the ratio De/Re being finite; to be precise, we examine finite values of the ratio (1-β)De/Re, defined as the elasticity number, where β is the ratio of the solvent viscosity to total viscosity. The limit De $\rightarrow \infty$ implies the effects of relaxation terms. We carryout a similar analysis for the Rankine vortex in chapter [3], again identifying the elastic continuous spectrum. In chapter [4], we retain the relaxation terms taking De to be large but finite and study the effects of relaxation terms on the continuous spectrum eigenfunctions. Finally in chapter [5], we conclude and provide a perspective on the future scope of the work.

Chapter 2

Elastic Coeutte flow

2.1 Introduction

An indication of the existence of a continuous spectrum governing the dynamics of small-amplitude perturbations in a shearing fluid in the inviscid limit was first given by Rayleigh (Rayleigh (1945)). An explicit spectral investigation in this regard was first carried out by Fjortoft and Hoiland (Fjortoft (1950)) for the special case of incompressible Couette flow. The explicit form of the continuous spectrum modes in the context of plasmas, where the linearized dynamics is governed by the Vlasov equation, was proposed by Van Kampen (Van Kampen (1955)), and extended to the hydrodynamic context by Case (Case (1960)) first for plane Couette flow. There have been several investigations since then of the continuous spectrum (CS) eigenfunctions in various scenarios, including non-linear base-state profiles, and the structure of the continuous spectrum eigenfunctions (CS-modes), in the inviscid limit ($Re \to \infty$), is now known in some detail for the case of parallel shear flows (Balmforth & Morrison (1995*b*); Sazonov (1989)), and swirling flows (Roy (2012)). The complete three-dimensional inviscid spectrum for an arbitrary plane parallel shearing flow has recently been obtained (Roy & Subramanian (2014*b*))

The linear stability of plane Couette flow in a viscoelastic fluid is a classical problem whose study originated with the seminal work of Gorodtsov and Leonov (GL) back in the 1960s (Gorodtsov & Leonov (1967)). Thereafter, several investigations on the underlying spectra of various flow profiles have been carried out under differing conditions(Miller (2005); Wilson *et al.* (1999); Kupferman (2005)). At zero Reynolds number (Re), the detailed spectrum is known for the upper-Convected Maxwell (UCM) (Gorodtsov & Leonov (1967); Wilson *et al.* (1999)) and the Oldroyd-B fluids (Kupferman (2005); Miller (2005)). For plane Couette flow of the UCM fluid, for any given streamwise wave number, in addition to a continuous spectrum, there exist two discrete eigenvalues. For plane Couette flow of the Oldroyd-B fluid, there are two continuous spectra, the one which is already there in the UCM case, the so-called Gorodtsov-Leonov (GL) spectrum, and a new viscous continuous spectrum which moves out to infinity as the retardation time tends to zero. Thus, the continuous spectrum is sensitive to the particular choice of constitutive model used, although its existence is insensitive to the particular base-state profile (Wilson *et al.* (1999)). However, it has also been shown that the nature of the discrete spectrum does depend on the base-state velocity profile.

In general, the detailed examination of the characteristics of the continuous spectrum has only been carried out in the inertialess limit. In the present study, we are interested in studying the nature of the continuous spectrum in the complementary (inertial) limit. Thus, the present investigation is focused on the regime $Re \to \infty$, $De \to \infty$ with the ratio $(1-\beta)De/Re$, known as the elasticity number E, being finite, where β is the ratio of the solvent viscosity to total viscosity; $\beta = 0$ denotes the UCM fluid and $\beta = 1$ denotes the Newtonian limit. Here, De is the ratio of the polymer relaxation time to time-scale of the flow, while Re is the ratio of the viscous to the flow time scale. We have $De = U\tau/L$ and $Re = \rho UL/\mu$, where τ is the microstructural relaxation time, U and L are the velocity and length scales characterizing the base-state profile, and ρ and μ are the density and total (solvent + polymer) viscosity, respectively.

The first investigation in the aforementioned limit ($De \to \infty$, E finite) was carried out by Azaiez & Homsy (1994) for the Oldroyd-B fluid, and there have been later investigations by Rallison and Hinch (Rallison & Hinch (1995)) and by Renardy and co-workers (Renardy (2008); Kaffel & Renardy (2010)) for the both the UCM and Oldroyd-B fluids. Note that the UCM and Oldroyd-B do not differ qualitatively with regard to their spectra in this limit since the solvent parameter β appears as a part of E; this is in sharp contrast to the inertialess limit where a new continuous spectrum (the viscous continuous spectrum) appears for any non-zero β. The governing equation for linearized perturbations in this limit is the so-called elastic Rayleigh equation. This equation has been examined earlier (Azaiez & Homsy (1994); Rallison & Hinch (1995); Renardy (2008)) with the emphasis being solely on the discrete modes. These discrete modes are either inertially unstable modes, associated with inflectional base-state profiles or free surfaces modified by elasticity (for the most part), or instabilities driven solely by elasticity and associated with a shear-driven resonance of elastic shear waves (Rallison & Hinch (1995); Reddy *et al.* (2015)). In contrast, we have made an attempt here to study the elastically modified continuous spectrum (CS-modes) in the inviscid limit. This being a first attempt, we focus on two canonical flow base-state profiles viz., plane Couette flow (this chapter) and the

Rankine vortex (the next chapter). Further, the effects of elasticity have been modelled based on the Oldroyd-B model (discussed in chapter[1]) in order to represent, in the simplest possible manner, the polymer-solvent coupling in a dilute polymer solution. For simple shear flow, the Oldroyd-B model predicts a constant shear viscosity and (positive) first normal stress difference, and a zero second normal stress difference, properties that are characteristic of Boger fluids. Before going into the details of the elastic analysis (non-zero E), we give a brief description of the inviscid analysis for each of Couette flow and the Rankine vortex at the beginning of the relevant chapters.

2.2 Problem formulation

Before proceeding to the asymptotic regime of interest ($De \rightarrow \infty$, E finite), we formulate the governing equations for arbitrary Re and De for plane Couette flow with the base-state velocity profile defined as $u_x = \dot{\gamma} y$, $\dot{\gamma}$ being the shear rate (the scale for the velocity gradient). These equations will be needed in chapter [4] where we examine the effects of a weak relaxation on the elastically modified continuous spectrum. If we define $\mathbf{F} = \nabla \cdot \sigma$, with σ being the polymeric stress field, as the elastic force acting on the fluid, then the equations governing the evolution of small amplitude perturbations in plane Couette flow can be written in the following non-dimensional form, in terms of the axial vorticity field (ω_z) and the (two) in-plane components of the elastic forces, as:

$$\Big(\frac{\partial}{\partial t} + y\frac{\partial}{\partial x}\Big)\omega_z = \frac{1}{Re}\nabla^2\omega_z + \frac{1}{Ma_e^2}(\nabla \wedge \mathbf{F})_z \tag{2.1}$$

$$\Big(\frac{\partial}{\partial t} + y\frac{\partial}{\partial x} + \frac{1}{De}\Big)F_x = F_y + (1+2De^2)\frac{\partial^2 u_x}{\partial x^2} + 2De\frac{\partial^2 u_x}{\partial x \partial y} + \frac{\partial^2 u_x}{\partial y^2} \tag{2.2}$$

$$\Big(\frac{\partial}{\partial t} + y\frac{\partial}{\partial x} + \frac{1}{De}\Big)F_y = (1+2De^2)\frac{\partial^2 u_y}{\partial x^2} + 2De\frac{\partial^2 u_y}{\partial x \partial y} + \frac{\partial^2 u_y}{\partial y^2} \tag{2.3}$$

where $\omega_z = (\frac{\partial u_y}{\partial x} - \frac{\partial u_x}{\partial y})$ with $F_x = (\frac{\partial \sigma_{xx}}{\partial x} + \frac{\partial \sigma_{xy}}{\partial y})$ and $F_y = (\frac{\partial \sigma_{xy}}{\partial x} + \frac{\partial \sigma_{yy}}{\partial y})$. The system of equations above is non-dimensionalized using the channel width b as the length scale, the inverse shear rate $\dot{\gamma}^{-1}$ as the time scale; thus, while the lower boundary is stationary, the upper boundary is moving with a speed $\dot{\gamma} b$. The non-dimensional numbers that appear in (2.4)-(2.7) are the Deborah number $De = \dot{\gamma}\tau$ (the ratio of the elastic relaxation to the flow time scale), the Reynolds number $Re = \dot{\gamma} b^2/\nu_s$ (the ratio of the viscous to the inertial time scale with ν being defined in terms of the total viscosity $\mu = \mu_p + \mu_s = (G\tau + \mu_s)$, and the elastic Mach number

$Ma_e = \dot{\gamma}b/c_{\text{elas}}$ with $c_{\text{elas}} = \sqrt{G/\rho}$ being the elastic shear wave speed in a quiescent elastic medium. Similar to its counterpart in compressible flows, Ma_e may be interpreted as the ratio of a characteristic flow velocity scale to the speed of propagation of infinitesimal amplitude shear stress (or vorticity) fluctuations in a quiescent incompressible elastic medium. Note that the elastic Rayleigh limit we examine below corresponds to the highly supersonic limit in the sense that $Ma_e \gg 1$.

Assuming a normal mode form, $f = \hat{f}(y)e^{i(kx-\omega t)}$, with $\omega = kc$, c being the phase speed of the mode, for the various perturbation quantities, we have:

$$\begin{aligned}
(y-c)(D^2-k^2)\hat{u}_y &= \frac{1}{ikRe}(D^2-k^2)^2\hat{u}_y + \frac{1}{Ma_e^2}(ik\hat{F}_y - D\hat{F}_x), && (2.4)\\
\Sigma_2\hat{F}_x &= \hat{F}_y - ik(1+2De^2)D\hat{u}_y - 2DeD^2\hat{u}_y + \frac{i}{k}D^3\hat{u}_y, && (2.5)\\
\Sigma_2\hat{F}_y &= -k^2(1+2De^2)\hat{u}_y + 2ikDeD\hat{u}_y + D^2\hat{u}_y, && (2.6)\\
\Sigma_2 &= -i\omega + iky + \frac{1}{De}. && (2.7)
\end{aligned}$$

On substituting equations for the elastic force terms in (2.4), we have a single fourth-order differential equation governing the perturbation normal velocity field ($\hat{u}_y$), given by:

$$\frac{1}{Ma_e^2}\Big(ik(\Sigma_2^2+2)A\hat{u}_y - \Big\{\frac{i}{k}\Sigma_2^2D^2 + 2\Sigma_2 D\Big\}A\hat{u}_y\Big) = (y-c)(D^2-k^2)\hat{u}_y - \frac{1}{ikRe}(D^2-k^2)^2\hat{u}_y, \tag{2.8}$$

where $A = D^2 + 2ikDeD - k^2(1+2De^2)$. This is the viscoelastic analog of the Orr-Sommerfeld equation that governs the stability of Newtonian fluids; the above equation has been examined earlier for $Re = 0$, in the context of plane parallel shearing flows, by Renardy & Renardy (1986) and Wilson *et al.* (1999). Following the footsteps of Gorodtsov & Leonov (1967), who used the above split-form of the original fourth order operator on the LHS to obtain analytical solutions in the inertialess limit, the above equation may be re-written in the form:

$$\begin{aligned}
\Rightarrow \quad & \Big[y_*^2D^2 - 2Dy_* + 2 - k^2y_*^2\Big]\Big[D^2 + 2ikDeD - k^2(1+2De^2)\Big]\hat{u}_y = \\
& -k^2Ma_e^2y_*^3\Big[(y-c)(D^2-k^2) - (ikRe)^{-1}(D^2-k^2)^2\Big]\hat{u}_y && (2.9)
\end{aligned}$$

where $y_* = \frac{\Sigma_2}{ik} = y - c - \frac{i}{kDe}$ and D=d/dy. The elastic Mach number may be written in terms of Re and De as $Ma_e^2 = \left(\frac{1}{1-\beta}\right)Re.De$. For a fixed β, the evolution of the perturbations, as governed by (2.4)-(2.7), depends therefore on Re and De, and (2.9) may be written in the form:

$$\Big[y_*^2D^2 - 2Dy_* + 2 - k^2y_*^2\Big]\Big[D^2 + 2ikDeD - k^2(1+2De^2)\Big]\hat{u}_y(y) =$$
$$-ikDe\Big(\frac{\beta}{1-\beta}\Big)y_*^3(D^2-k^2)^2\hat{u}_y - k^2(Re.De)\Big(\frac{\beta}{1-\beta}\Big)y_*^3(y-c)(D^2-k^2)\hat{u}_y(y). \quad (2.10)$$

2.2.1 The continuous spectrum for finite Re and De

Apart from discrete modes, for any finite De and Re, (2.10), supports a pair of continuous spectra. In general, since the continuous spectra are associated with the regular singularities of the governing ODE, the relevant solutions near these points may involve logarithms and/or fractional powers (making them multi-valued in the complex plane). For, this reason, continuous spectra usually appear as branch cuts of the dispersion relation that governs the eigenvalues. In the present case, the pair of continuous spectra is given by $y\epsilon y_c$ with the y_c intervals being defined by:

$$\Sigma_2(y_c) = 0 \quad (2.11)$$
$$\Sigma(y_c) + \frac{i}{\beta De} = 0 \quad (2.12)$$

where Σ_2(y) and $\Sigma(y)$. For Re $=\infty$, there also arises the well-known inviscid continuous spectrum (CS), given by $\Sigma(y_c) = 0$, and spanning the base-state range of velocities. However, with Re finite and for a bounded domain, the continuous spectra arise solely due to the additional viscoelastic terms in (2.10).

The relation (2.12) defines the so-called Gorodtsov-Leonov (GL) continuous spectrum (Gorodtsov & Leonov (1967)) named after the authors who first examined viscoelastic plane Couette flow of a UCM fluid for finite De. Although usually studied in the aforementioned specific context owing to its analytical tractability (Graham (1998)), the GL spectrum continues to exist for finite Re, and for both parallel shear flows and azimuthal shearing flows (see next chapter on the elastic Rankine vortex). The singular GL-eigenfunctions, in addition to being convected with the flow velocity at y = y$_c$, decay at a rate De^{-1} due to relaxation, asymptoting to neutral stability for $De \to \infty$. For the case of plane parallel flows, the GL spectrum is characterized by the integer Frobenius exponents 0, 1, 3 and 4 (Wilson *et al.* (1999); Kupferman (2005)).

An additional continuous spectrum, given by (2.12) arises due to a finite solvent viscosity (Wilson *et al.* (1999)), being is pushed off to infinity in the UCM limit ($\beta \to 0$). Th CS-eigenfunctions in this case have Frobenius exponents 0, 1, 2 and $3-2/\beta$. As noted by Kupferman (2005), the final Frobenius exponent is in general fractional, and indicates the existence of an algebraic branch point and an associated branch cut. The CS-eigenfunctions in this case require therefore a principal-finite-part interpretation (Engevik (1971); Roy & Subramanian (2014*a*); Reddy *et al.* (2015)).

2.3 Elastic Rayleigh equation (Re→ ∞ and De→ ∞)

We now proceed to the regime of interest, $De \to \infty$, $Re \to \infty$ with $E = \frac{De^2}{Ma^2}$ fixed, in which case the neglect of the $O(De^{-1})$ terms denoting microstructural relaxation, yields the following equation governing $\hat{u}_y$:

$$(y-c)^4\left[D^2-k^2\right]\hat{u}_y(y) = 2E\Big[(y-c)^2(D^2-k^2) - 2(y-c)D + 2\Big]\hat{u}_y(y) \tag{2.13}$$

One has to note that (2.13), is equivalent to (18) in Azaiez & Homsy (1994). Thus, the original fourth order ODE equation resulting from (2.4)-(2.7), reduces to a second-order ODE in the limit $De \to \infty$, E, β fixed, implying that the neglect of relaxation is a singular limit. From what is known for the eigenfunctions of the Rayleigh and Orr-Sommerfeld equations (see section 5 in Roy & Subramanian (2014*b*)), one expects a non-trivial relationship between the spectrum of the elastic Rayleigh equation, and that for large but finite De. As noted earlier, the viscosity ratio β no longer plays a fundamental role (for finite De, a non-zero β led to an additional continuous spectrum), since, in the above limit, one may interpret a change in β in terms of a re-scaled E.

For an arbitrary flow, the elastic Rayleigh equation (ERE) takes the following form (Rallison & Hinch (1995)):

$$\frac{d}{dy}\left[(\rho(U-c)^2 - GA_{11})\frac{d}{dy}\frac{\phi}{U-c}\right] = (\rho(U-c)^2 - GA_{11})\frac{\alpha^2\phi}{U-c}, \tag{2.14}$$

The variable ϕ in the above equation represents the perturbation stream with $\phi(y) = \frac{i}{k}\hat{u}_y(y)$. On expanding (2.14) we have:

$$(U-c)^4\left\{(D^2-k^2) - \frac{U''}{U-c}\right\}\phi = \frac{G}{\rho}\left[A_{11}\left\{(U-c)^2(D^2-k^2) - (U-c)U'' - 2U'(U-c)D + U'^2\right\}\right.$$
$$\left. + A'_{11}\left\{(U-c)^2D - U'(U-c)\right\}\right]\phi \tag{2.15}$$

For the plane Couette case, with $U(y) = y$, $E = \frac{GA_{11}}{\rho}$, $A_{11} = 1 + 2\tau^2$ and $c = y_c$, and the above equation reduces to (2.13). One may note that (2.14), is in the self-adjoint form in terms of the normal displacement ψ, defined as $\psi = \frac{\phi}{U-c}$. Hence, one can easily construct the following modified version of Howard semi-circle theorem (Rallison & Hinch (1995); Miller (2005); Kaffel & Renardy (2010)) for parallel flows:

$$\left\{c_r - \left(\frac{u_{max} + u_{min}}{2}\right)\right\}^2 + c_i^2 \leq \left(\frac{u_{max} + u_{min}}{2}\right)^2 - 2E(u')^2_{min} \tag{2.16}$$

As seen from (2.16), the role of elasticity is to shrink the inviscid semi-circle of instability, implying a relative stabilization. The mechanism of instability associated with the original Rayleigh equation requires an inflection point, and may be interpreted in terms of the resonant interaction of vorticity waves (M.E.McIntyre & Weissman (1978)). An additional mechanism of instability, associated with the elastic Rayleigh equation, is that resulting from the resonant interaction of a pair of elastic shear waves (the balance between inertia and elasticity supports the propagation of such waves). The shear waves propagate more rapidly (relative to the flow) with increasing E, and the onset of absolute stability coincides with the inability of the base-state shear, beyond a threshold E, to bring a pair of such waves into resonance by causing them to propagate at the same speed (Renardy (2008)).

Further analysis shows that (2.13) has two regular singularities at the locations $y = y_c \pm \sqrt{2E}$ which correspond to the locations of the two travelling shear wave singularities; $y = y_c$ corresponds to the critical level singularity. Since all singular points are regular, a local expansion of solutions can be found using Frobenius theory. At the travelling wave singularities ($y_c \pm \sqrt{2E}$), both Frobenius indices are 0; as a result, one of the solutions approaches a constant and the other diverges logarithmically. At the critical level ($y = y_c$), the Frobenius indices are integers (1 and 2).

It is worth noting that, for arbitrary E, the elastic Rayleigh equation belongs to the confluent Heun class (Slavyanov & Lay (2000); Renardy (2008)) making any sort of analysis difficult. We therefore examine analytically the effects of elasticity on the continuous spectrum in the limit of small but finite E. Even for small E, elasticity plays an important role in the vicinity of the critical level, and the analysis that follows is therefore based on a matched asymptotic expansions approach. The inertial terms become vanishingly small close to the critical level ($y = y_c$) due to the vanishing Doppler frequency ($\Sigma = ik(y - y_c) = 0$). The elastic terms, however, remain finite since the base-state shear (which controls the polymeric stresses) at the critical level remains finite. As a result, with the addition of elasticity, there exists a region with a thickness of $O(\sqrt{E})$ about the critical level, where elasticity and inertia are comparable. Thus, the flow domain may be divided into two regions in the general case an interior boundary layer (inner) region where inertia and elasticity are of the same order and outer regions which are dominated by inertia (see Figure(2.1)).

2.4 Boundary layer analysis of the (elastic Rayleigh equation) for small but finite E

2.4.1 The outer solutions

We now describe the analysis in the individual regions mentioned above, and the undetermined constants are then determined through a matching procedure. Towards this end, we shall take a step back to study the inviscid CS-modes which comes handy for the elastic analysis. The structure of the inviscid continuous spectrum modes for plane Couette flow was originally derived by Case (Case (1960)), and the plane Couette profile being a degenerate instance of a non-inflectional profile with $U(y) = y$, the spectrum is purely continuous. We consider plane Couette flow between boundaries at $y = 0$ and $y = 1$, with the plate at $y = 1$ moving parallel to itself with unit velocity; as before, x and y refer to the streamwise and gradient directions. Assuming a normal mode form, $g = \hat{g}(y)e^{i(kx-\omega t)}$, one arrives at the Rayleigh equation governing the linearized evolution the normal velocity eigenfunction $\hat{u}_y(y)$ originally considered by Case (Case (1960)):

$$(y - y_c)[D^2 - k^2]\hat{u}_y(y) = 0, \tag{2.17}$$

corresponding to setting $E = 0$ in (2.13). The above equation has kinked solutions of the form (see Figure(2.1)):

$$\begin{aligned}
\hat{u}_{y1}(y; y_c) &= -\frac{\sinh[k(1-y_c)]\sinh[ky]}{k\sinh k} = A^{(-)}\sinh[ky] \quad \text{for} \quad 0 < y < y_c, && (2.18)\\
\hat{u}_{y2}(y; y_c) &= -\frac{\sinh[ky_c]\sinh[k(1-y)]}{k\sinh k} = A^{(+)}\sinh[k(1-y)] \quad \text{for} \quad y_c < y < 1. && (2.19)
\end{aligned}$$

where $A^{(-)} = \frac{\sinh[k(1-y_c)]}{k\sinh k}$, $A^{(+)} = \frac{\sinh[ky_c]}{k\sinh k}$ and $D = d/dy$, and which satisfy the condition of zero normal velocity at the boundaries. The location where $y = y_c$, corresponding to the kink, is termed the 'critical level', the kink being a jump in the slope across the critical level; it is the location in the flow domain where the phase speed of the perturbation equals the base-state velocity. The vorticity eigenfunction corresponding to the above CS-mode turns out to be a vortex sheet, being given by a Dirac-delta-function singularity at the critical level. Hence, the inviscid eigenfunctions are vortex sheets convected by the base-state flow and amplitude of the vortex-sheet remaining non-zero over the entire range of wave speeds.

For non-zero E, (2.17) constitutes the leading-order approximation for the eigenfunction away from the critical level. The elastic terms become comparable close to the critical level. As a result, the original critical level, loosely speaking, spreads out into an $O(E^{\frac{1}{2}})$ elastic boundary layer localized around $y = y_c$ where the velocity and stress fields are governed by a balance of inertia and elasticity. To analyze the problem in the framework of matched asymptotic expansion, we now introduce a boundary layer (BL) variable ξ, defined as

$$\xi = \frac{y - y_c}{\sqrt{2\mathrm{E}}} \tag{2.20}$$

On substituting in (2.13), with the transformation of variable from 'y' to ξ, we have:

$$\left[\xi^2(\xi^2-1)\frac{d^2}{d\xi^2} + 2\xi\frac{d}{d\xi} - 1 - E[k\xi^2(\xi^2-1])\right]\tilde{u}_y(\xi) = 0 \tag{2.21}$$

within an $O(E^{\frac{1}{2}})$ boundary layer around the critical level.

Now, considering the inner expansion $\tilde{u}_y(\xi) = \tilde{u}_y^{(0)}(\xi) + \sqrt{E}\tilde{u}_y^{(1)}(\xi) + \cdots$, one obtains from (2.21) the following governing equation at leading order:

$$\left[\xi^2(\xi^2-1)D^2 + 2\xi D - 2\right]\tilde{u}_y^{(0)} = 0, \tag{2.22}$$

the solution of which is given by:

$$\tilde{u}_y^{(0)}(\xi) = B_1\xi + B_2\xi\ln\left|\frac{\xi-1}{\xi+1}\right|, \tag{2.23}$$

The values $\xi = \pm 1$ denote the locations of the travelling wave singularities (the travelling waves referred to in earlier sections), where the normal velocity is logarithmically divergent (contrast

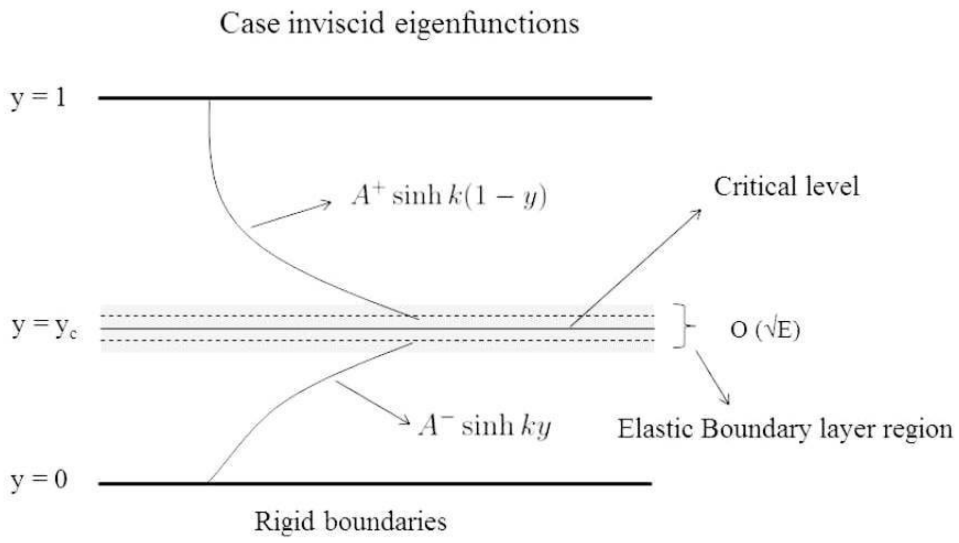

Figure 2.1: Distribution of different regions in Couette flow

this with the purely inviscid case where the normal velocity remains finite at the critical level), and they divide the elastic boundary layer into three distinct regions. The solution forms in the individual regions may be written explicitly as:

$$\tilde{u}^{(0)}_{y-}(\xi) = \xi\Big[B_1^- + B_2 \ln\left|\frac{\xi-1}{\xi+1}\right|\Big] \quad \xi < -1 \tag{2.24}$$

$$\tilde{u}^{(0)}_{y}(\xi) = \xi\Big[B_1 + B_2 \ln\frac{1-\xi}{1+\xi}\Big] \quad -1 < \xi < 1 \tag{2.25}$$

$$\tilde{u}^{(0)}_{y+}(\xi) = \xi\Big[B_1^+ + B_2 \ln\frac{\xi-1}{\xi+1}\Big] \quad \xi > 1 \tag{2.26}$$

Note that we have chosen the same constant for the singular logarithmic solution in all three parts of the boundary layer with the logarithm being real valued in each region. This choice is consistent with the purely inviscid case ($E = 0$) where, for a general non-linear shear flow, the constant multiplying the logarithmically singular Tollmein solution is the same across the critical level, and it is the jump in the constant multiplying the regular solution that generates the inviscid CS-spectrum of the Rayleigh equation (Balmforth & Morrison (1995*b*)). It will be seen below that the constants in the two peripheral regions ($B_1^{\pm}, B_2$) are constrained by matching, and an appropriate choice can accommodate the differing slopes of the outer solutions on either side. The regular constant in the central part of the boundary layer, at leading (B_1) and higher orders, can be chosen independently, however, and this additional degree of freedom is crucial to the existence of additional continuous spectra for any finite E.

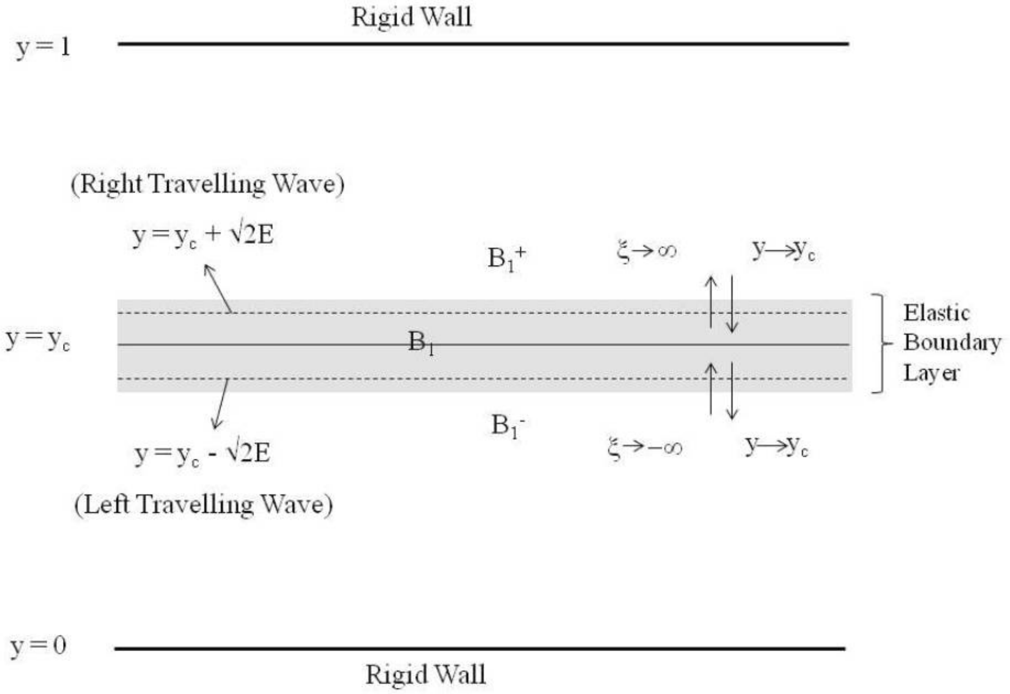
Rigid Wall
y = 1
(Right Travelling Wave)
y = y_c + √2E
B_1^+
ξ→∞
y→y_c
y = y_c
B_1
Elastic Boundary Layer
B_1^-
ξ→−∞
y→y_c
y = y_c - √2E
(Left Travelling Wave)
y = 0
Rigid Wall

Figure 2.2: Matching in Couette flow

2.4.2 Matching the inner (boundary layer) and the outer solutions

We now match the inner boundary layer (BL) solutions to the outer inviscid solutions, following the matching requirement given by:

$$\tilde{u}^{(i)}_{y-}(\xi)|_{\xi\to-\infty} \quad \Leftrightarrow \quad \hat{u}^{(i)}_{y1}(y)|_{y\to y_c^-} \tag{2.27}$$

$$\tilde{u}^{(i)}_{y+}(\xi)|_{\xi\to\infty} \quad \Leftrightarrow \quad \hat{u}^{(i)}_{y2}(y)|_{y\to y_c^+} \tag{2.28}$$

The far-field forms of the inner solutions are given by:

$$\begin{aligned}\tilde{u}^{(0)}_{y+}(\xi)|_{\xi\to\infty} &= B_1^+\xi - 2B_2,\\ \tilde{u}^{(0)}_{y-}(\xi)|_{\xi\to-\infty} &= B_1^-\xi - 2B_2.\end{aligned} \tag{2.29}$$

The near-Field forms of the outer solutions are given by:

$$\hat{u}_{y1}^{(0)}(y;y_c)|_{y\to y_c} = A_0^{(-)}\Big[\sinh[ky_c] + \sqrt{2E}(k\xi)\cosh[ky_c]\Big] + \cdots \tag{2.30}$$

$$\hat{u}_{y2}^{(0)}(y;y_c)|_{y\to y_c} = A^{(+)}\Big[\sinh[k(1-y_c)] - \sqrt{2E}(k\xi)\cosh[k(1-y_c)]\Big] + \cdots \tag{2.31}$$

On matching the limiting forms of the inner and outer solutions above, we have the following relations:

$$B_1^- = A^{(-)}(k\sqrt{2E})\cosh[ky_c] \tag{2.32}$$

$$B_1^+ = -A^{(+)}(k\sqrt{2E})\cosh[k(1-y_c)] \tag{2.33}$$

$$B_2 = -\frac{A^{(+)}\sinh[k(1-y_c)]}{2} \quad \text{or} \quad -\frac{A^{(-)}\sinh[ky_c]}{2} \tag{2.34}$$

The form of the normal velocity eigenfunction within the elastic boundary layer may be written in following way:

$$\tilde{u}_y^-(\xi) = \xi A^{(-)}\Big[k(2E)^{1/2}\cosh[ky_c] - \frac{\sinh[ky_c]}{2}\text{Pf.}\ln\left|\frac{\xi-1}{\xi+1}\right|\Big] \quad \xi < -1, \tag{2.35}$$

$$\tilde{u}_y(\xi) = \xi\Big[B_1 - \frac{A^{(-)}\sinh[ky_c]}{2}\text{Pf.}\ln(\frac{1-\xi}{1+\xi})\Big] \quad -1 < \xi < 1, \tag{2.36}$$

$$\tilde{u}_y^+(\xi) = -\xi A^{(+)}\Big[k(2E)^{1/2}\cosh[k(1-y_c)] + \frac{\sinh[k(1-y_c)]}{2}\text{Pf.}\ln(\frac{\xi-1}{\xi+1})\Big] \quad \xi > 1, \tag{2.37}$$

where B_1 is still arbitrary, and the prefix Pf. in (2.35)-(2.37) denotes a principal-finite-part interpretation which, as will be seen below, is required in interpreting the vorticity field within elastic boundary layer. With the complete solution forms for the normal velocity eigenfunction over the entire domain at hand, we now study the structure of the perturbation vorticity field in the next section.

2.4.3 Perturbation vorticity field

For the inviscid case (E = 0), as discussed earlier the vorticity field is a delta function at $y = y_c$ with the vortex sheet strength being an $O(1)$ quantity. For small but finite E, the vorticity field is still localized in the elastic boundary layer which may be regarded as a vortex sheet on the scale of the outer region. The perturbation vorticity eigenfunction in terms of the normal velocity, $\hat{u}_y(y; y_c)$, is given by:

$$
\begin{aligned}
\hat{\omega}_z(y) &= -\nabla^2\psi, && (2.38)\\
&= -\frac{i}{k}[\nabla^2(\tilde{u}_y)], && (2.39)\\
\Rightarrow \hat{\omega}_z(y) &= \frac{i}{k}\Big[-\frac{\partial^2\tilde{u}_y}{\partial y^2} + k^2\tilde{u}_y\Big] && (2.40)
\end{aligned}
$$

where ψ is the stream function and ∇^2 denotes the Laplacian. The total vorticity associated with the above eigenfunction is:

$$
\omega_z(y) = \int_{y_c-O(1)}^{y_c+O(1)} \hat{\omega}_{z(y)}dy. \tag{2.41}
$$

On considering $\xi = \frac{y-y_c}{\sqrt{2E}}$, and transforming the variable, we have:

$$
\omega_z(\xi) = \int_{-\infty}^{+\infty} \hat{\omega}_z(\xi)(2E)^{1/2}d\xi \tag{2.42}
$$

where

$$
\tilde{\omega}_z(\xi) = 2E\hat{\omega}_z(\xi) \quad \text{and} \quad \tilde{\omega}_z(\xi) = \Big[-\frac{i}{k}\Big(\frac{\partial^2\tilde{u}_y}{\partial\xi^2}\Big) + E(2ik)\tilde{u}_y\Big]. \tag{2.43}
$$

Substituting in (2.43) for the scaled vorticity eigenfunction, we have the following expression for leading order vorticity field:

$$
\begin{aligned}
\tilde{\omega}_z^{(0)}(\xi) &= -\frac{i}{k}\Big[\frac{\partial^2\tilde{u}_y^{(0)}}{\partial\xi^2}\Big], && (2.44)\\
&= \frac{i}{k}\Big[-\text{Pf.}\frac{4B_2}{(\xi^2-1)^2} + B_1[\delta(\xi+1) - \delta(\xi-1) + \delta'(\xi+1) + \delta'(\xi-1)]\Big] && (2.45)
\end{aligned}
$$

The integrated boundary-layer vorticity, for small E, is therefore given by:

$$
\begin{aligned}
\omega_z(\xi) &= \sqrt{E}\Big(\int_{-\infty}^{+\infty} \tilde{\omega}_z^{(0)}(\xi)\sqrt{2}d\xi\Big) + O(E) && (2.46)\\
&= -\frac{4iB_2}{k(2E)^{1/2}} \quad \text{Pf.}\int_{-\infty}^{+\infty} \frac{d\xi}{(\xi^2-1)^2} + (B_1^+ - B_1^-), && (2.47)\\
&= B_1^+ - B_1^-, && (2.48)
\end{aligned}
$$

since the principal-finite-part integral is identically zero. Thus, the boundary layer vorticity continues to be $O(1)$ in the limit $E \ll 1$, and therefore consistent with the purely inviscid limit.

2.4.4 Uniformly valid analysis

In equations (2.35)-(2.37), there are two arbitrary parameters, the amplitude parameter A in the outer solution (recall that both $A^{(-)}$ and $A^{(+)}$ in (2.35)-(2.37) are proportional to A), already present in the purely inviscid limit, and the parameter B_1 in the central part of the elastic boundary layer (that remained undetermined in the above analysis). This implies that the expressions (2.35)-(2.37) actually combine two one-parameter continuous spectrum families. It is convenient to characterize each of these families separately by appropriate choices for the constant B_1, so that the expressions (2.35)-(2.37), for an arbitrary B_1, correspond to a linear superposition of the two families each of which is parameterized by A alone. The two choices for B_1 are evident from (2.35)-(2.37). The first family may be taken as corresponding to $B_1 = A^{(-)}k(2E)^{\frac{1}{2}}\cosh[ky_c]$ while the second corresponds to $B_1 = -A^{(+)}k(2E)^{\frac{1}{2}}\cosh[k(1-y_c)]$. These choices help resolve the kink in the regular boundary layer solution across $\xi = -1$ and $\xi = 1$, respectively, and the boundary layer eigenfunctions in the two finite-E continuous spectrum families may therefore be written as:

$$\tilde{u}_{y-}(\xi) = \hat{B}_2\text{Pf.}\xi\ln\frac{\xi-1}{\xi+1} + (2E)^{\frac{1}{2}}\xi\hat{B}_{1-} \quad \xi < -1, \tag{2.49}$$

$$\tilde{u}_{y+}(\xi) = \hat{B}_2\text{Pf.}\xi\ln\left|\frac{\xi-1}{\xi+1}\right| + (2E)^{\frac{1}{2}}\xi\hat{B}_{1+} \quad \xi > -1, \tag{2.50}$$

and,

$$\tilde{u}_{y-}(\xi) = \hat{B}_2\text{Pf.}\xi\ln\left|\frac{\xi-1}{\xi+1}\right| + (2E)^{\frac{1}{2}}\xi\hat{B}_{1-} \quad \xi < 1, \tag{2.51}$$

$$\tilde{u}_{y+}(\xi) = \hat{B}_2\text{Pf.}\xi\ln\frac{\xi-1}{\xi+1} + (2E)^{\frac{1}{2}}\xi\hat{B}_{1+} \quad \xi > 1, \tag{2.52}$$

respectively. The first pair of expressions have a kink at $\xi = -1$ alone, corresponding to the shear wave travelling at a speed $(2E)^{\frac{1}{2}}$ faster than the base-state velocity at $y = y_c$. Terming this as the 'slow shear wave', the expressions (2.49)-(2.50), together with those in the outer region, may be said to correspond to the slow-shear-wave continuous spectrum, henceforth abbreviated as the $SSWS$. By the same reasoning, the second pair of expressions (2.51)-(2.52) correspond to the fast shear wave, and may be termed the fast-shear-wave spectrum abbreviated as the SSWS. Note that it is the kink in the regular solution across either of the travelling wave locations that allows for the satisfaction of the boundary conditions for an arbitrary y_c within a given interval, leading to a continuous spectrum. Thus, the continuous spectrum intervals corresponding to the

$FSWS$ and the $SSWS$ may be obtained from requiring that the location of the kink be in the physical domain (that is, between $y = 0$ and $y = 1$). The kink at $\xi = -1$ will lie in the domain provided y_c lies in the interval $[(2E)^{\frac{1}{2}}, 1 + (2E)^{\frac{1}{2}}]$ which yields the SSWS spectrum; a similar requirement for the kink at $\xi = 1$ leads to the FSWS interval being given by $[-(2E)^{\frac{1}{2}}, 1-(2E)^{\frac{1}{2}}]$.

Clearly, for finite E, the continuous spectrum intervals extend outside the base-state interval of velocities, in apparent violation of the finite-E generalization of the Howard semi-circle theorem. In the matched asymptotic expansions approach above, it has implicitly been assumed that the elastic boundary layer is in the interior of the domain, or in other words, the 'edges' of the boundary layer are at distances from the two boundaries that are much greater than $O(E^{\frac{1}{2}})$. In such a case, the impenetrability conditions at the boundaries may be imposed on the outer solutions, which are then given by (2.18) and (2.19). However, once the elastic boundary layer is within a distance of $O(E^{\frac{1}{2}})$ from either boundary, the wall boundary conditions need to applied to a uniformly valid solution constructed from both the inner (boundary layer) and outer solutions; rather than the outer solution alone. Such a uniformly valid solution is a composite structure that reduces to different (inner and outer) forms in the respective limits, and is needed when resolving the continuous spectrum eigenfunctions within a distance of $O(E^{\frac{1}{2}})$ from the ends of the $FSWS$ and $SSWS$ intervals (those eigenfunctions that exist in violation of the Howard semi-circle theorem). Note that one only need to account for one boundary at a time when constructing the uniformly valid solution since the elastic boundary layer remains an $O(1)$ distance away from the other.

Uniform solution near the lower boundary ($y = 0$):

We use 'additive composition' given in Dyke (1975) to construct the composite or uniformly valid solution. In this method, we take the sum of the inner and outer expansions and subtract the part they have in common to prevent double counting. We start from a different form for the inviscid outer solution ($\hat{u}_y(y; y_c)$) governed by (2.17), of the form $(e^{ky} + b'e^{-ky})$. On matching the asymptotic form of the above defined outer inviscid solution to the one in (2.29), we have following relation for the inner constants:

$$\begin{aligned} B_1^- &= k(2E)^{1/2}(e^{ky_c} - b'e^{-ky_c}) \\ B_2^- &= -\frac{e^{ky_c} + b'e^{-ky_c}}{2} \end{aligned} \tag{2.53}$$

The overlapping component of the inner and outer solutions is given by, $-2B_2^- + \xi B_1^-$. Hence, we have the following expression for the uniform solution near inner wall (y=0):

$$u_y^{(-)}(y) = e^{ky} + b'e^{-ky} + \Big(\frac{y-y_c}{\sqrt{2E}}\Big)\Big[B_1^- + B_2^- \log\left|\frac{y-y_c+\sqrt{2E}}{y-y_c-\sqrt{2E}}\right|\Big] + 2B_2^- - \Big(\frac{y-y_c}{\sqrt{2E}}\Big)B_1^- \tag{2.54}$$

One can see that in the limit $(y-y_c) \to O(\sqrt{E})$, the above solution takes the form of the outer inviscid solution and for the case $(y-y_c) \to O(1)$, it reduces to the inner boundary layer solution. Now, applying the boundary condition, $u_y^-(0) = 0$ to the above expression, and using (2.53), we have:

$$b' = -\frac{\Big(1 - e^{ky_c} + \frac{y_c e^{ky_c}}{2\sqrt{2E}} \log\left|\frac{y_c-\sqrt{2E}}{y_c+\sqrt{2E}}\right|\Big)}{\Big(1 - e^{-ky_c} + \frac{y_c e^{-ky_c}}{2\sqrt{2E}} \log\left|\frac{y_c-\sqrt{2E}}{y_c+\sqrt{2E}}\right|\Big)} \tag{2.55}$$

One can easily verify that the above expression in the limit $(y-y_c) \approx O(1)$, reduces to -1 which led to the simplified expression (2.18). The complete expression for the uniformly valid solution in the region $(0, y_c - \sqrt{2E})$ is given by,

$$u_y^{(-)}(y) = \Big\{e^{ky} - e^{ky_c} - \frac{(y-y_c)e^{ky_c}}{2\sqrt{2E}} \log\left|\frac{y-y_c+\sqrt{2E}}{y-y_c-\sqrt{2E}}\right|\Big\} \tag{2.56}$$

$$+b'\Big\{e^{-ky} - e^{-ky_c} - \frac{(y-y_c)e^{-ky_c}}{2\sqrt{2E}} \log\left|\frac{y-y_c+\sqrt{2E}}{y-y_c-\sqrt{2E}}\right|\Big\} \tag{2.57}$$

where b' is given by (2.55).

Uniform solution near the upper boundary $(y = 1)$:

From matching the outer solutions to the relevant inner solutions, we have:

$$\begin{aligned} B_1^+ &= k(2E)^{1/2}(e^{ky_c} - b'e^{-ky_c}) \\ B_2^+ &= -\frac{e^{ky_c} + b'e^{-ky_c}}{2} \end{aligned} \tag{2.58}$$

Therefore, the expression for the uniformly solution valid in the region $(y_c + \sqrt{2E}, 1)$, is given by:

$$u_y^{(+)}(y) = e^{ky} + b'e^{-ky} + \Big(\frac{y-y_c}{\sqrt{2E}}\Big)\Big[B_1^+ + B_2^+ \log\Big(\frac{y-y_c-\sqrt{2E}}{y-y_c+\sqrt{2E}}\Big)\Big] + 2B_2^+ - \Big(\frac{y-y_c}{\sqrt{2E}}\Big)B_1^+ \tag{2.59}$$

For the above solution to satisfy the boundary condition $u_y^{(+)}(1) = 0$, one requires:

$$\Rightarrow b' = -\frac{\left(e^{k} - e^{ky_c} - \frac{(1-y_c)e^{ky_c}}{2\sqrt{2E}}\log\left(\frac{1-y_c-\sqrt{2E}}{1-y_c+\sqrt{2E}}\right)\right)}{\left(e^{-k} - e^{-ky_c} - \frac{(1-y_c)e^{-ky_c}}{2\sqrt{2E}}\log\left(\frac{1-y_c-\sqrt{2E}}{1-y_c+\sqrt{2E}}\right)\right)} \tag{2.60}$$

For $(y-y_c) \to O(\sqrt{E})$, the above expression takes the value $-e^{2k}$, which led to the simpler expression (2.19). Hence the complete expression for the uniform solution in the region $(y_c + \sqrt{2E}, 1)$ is given by,

$$\begin{aligned} u_y^{+}(y) &= \left\{e^{ky} - e^{ky_c} - \frac{(y-y_c)e^{ky_c}}{2\sqrt{2E}}\log\left(\frac{y-y_c-\sqrt{2E}}{y-y_c+\sqrt{2E}}\right)\right\} &\quad (2.61)\\ &\quad + b'\left\{e^{-ky} - e^{-ky_c} - \frac{(y-y_c)e^{-ky_c}}{2\sqrt{2E}}\log\left(\frac{y-y_c-\sqrt{2E}}{y-y_c+\sqrt{2E}}\right)\right\} &\quad (2.62) \end{aligned}$$

with b' given by (2.60).

2.5 Numerical results

In this section we study numerically the spectrum of the elastic Rayleigh equation with Couette flow as the base-state velocity profile. For this purpose, we adopt a standard spectral method based on a Chebyshev collocation given in Trefethen (2000). There are difficulties with this method arising from the presence of continuous spectra. Since the continuous spectrum modes are not C^{∞}, there is in general a ballooning of the numerical spectrum for any finite number (N) of collocation points, resulting in the numerically determined eigenvalues having spurious imaginary parts (both positive and negative values arise owing to the time reversibility of the Rayleigh equation). Note that this ballooning is a strong function of how singular a given eigenfunction is; thus, the purely inviscid ($E = 0$) normal velocity eigenfunctions, where the singularity is only a jump in slope, do not lead to ballooning. The ballooned finite-E spectrum does collapse onto the real axis, albeit at a slow rate, with increasing N. This is seen from the plots shown in figure (2.3), where the numerical balloon clearly shrinks with increasing N (despite the increase in the number of spurious modes), the decrease scaling roughly as $1/N$.

We nevertheless use the spectral results to verify the predicted theoretical bounds for the travelling-wave spectra identified in the earlier section. The spatial extent of the numerical spectrum, projected onto the real axis, remains independent of N and the aforementioned ballooning tendency. Thus, verification of the changing continuous spectrum interval, with varying E, does

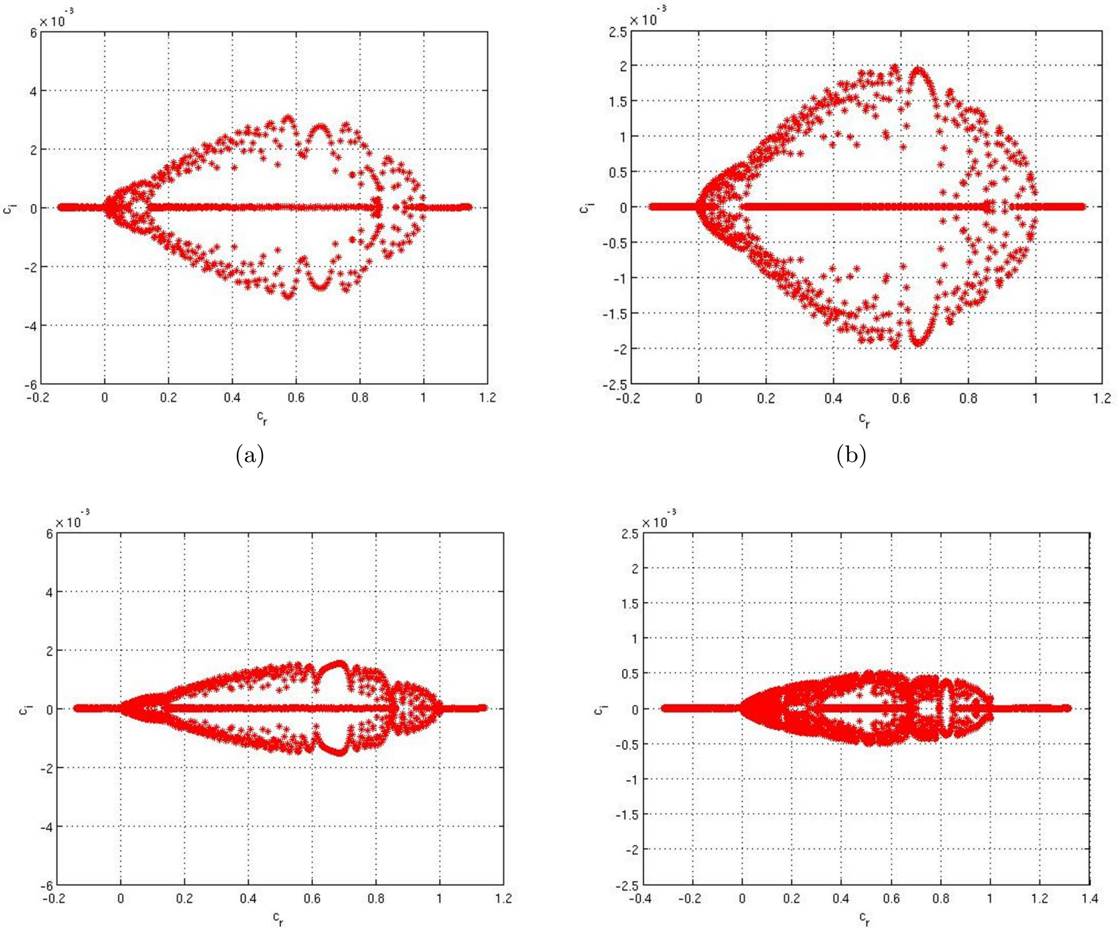

(a) (b) (c) (d)

Figure 2.3: Elastic Couette flow spectrum with ‘E(=0.01)’ fixed .(a) N=300 (b) N=450 (c) N=600 (d) N=1200

not pose a problem and is shown in figure (2.4) where the spectral interval is seen to run from $-(2E)^{\frac{1}{2}}$ to $1 + (2E)^{\frac{1}{2}}$. Three continuous spectra make up this interval. Although not analyzed in the earlier sections, the third continuous spectrum is one associated with the critical level, the original Doppler spectrum modified by elasticity, and corresponding to the base-state interval of velocities: $y_c \, \epsilon \, (0, 1)$.

The ballooning in the plots in figure (2.4) is affected by the overlap of the multiple (three) continuous spectra which leads to more singular eigenfunctions (simultaneous presence of both travelling-wave singularities and the critical-level singularity). For $E < 0.1$, there is a central interval where all three spectra ($FSWS$, $SSWS$ and Doppler) overlap and a pair of peripheral regions where two ($FSWS$+ Doppler; $SSWS$+ Doppler) overlap; this leads to a roughly three-fold structure for the spectral balloon, the ballooning being distinctly greater in the central portion. In the range $0.1 < E < 0.5$, the spectral balloon has a two-fold structure corresponding

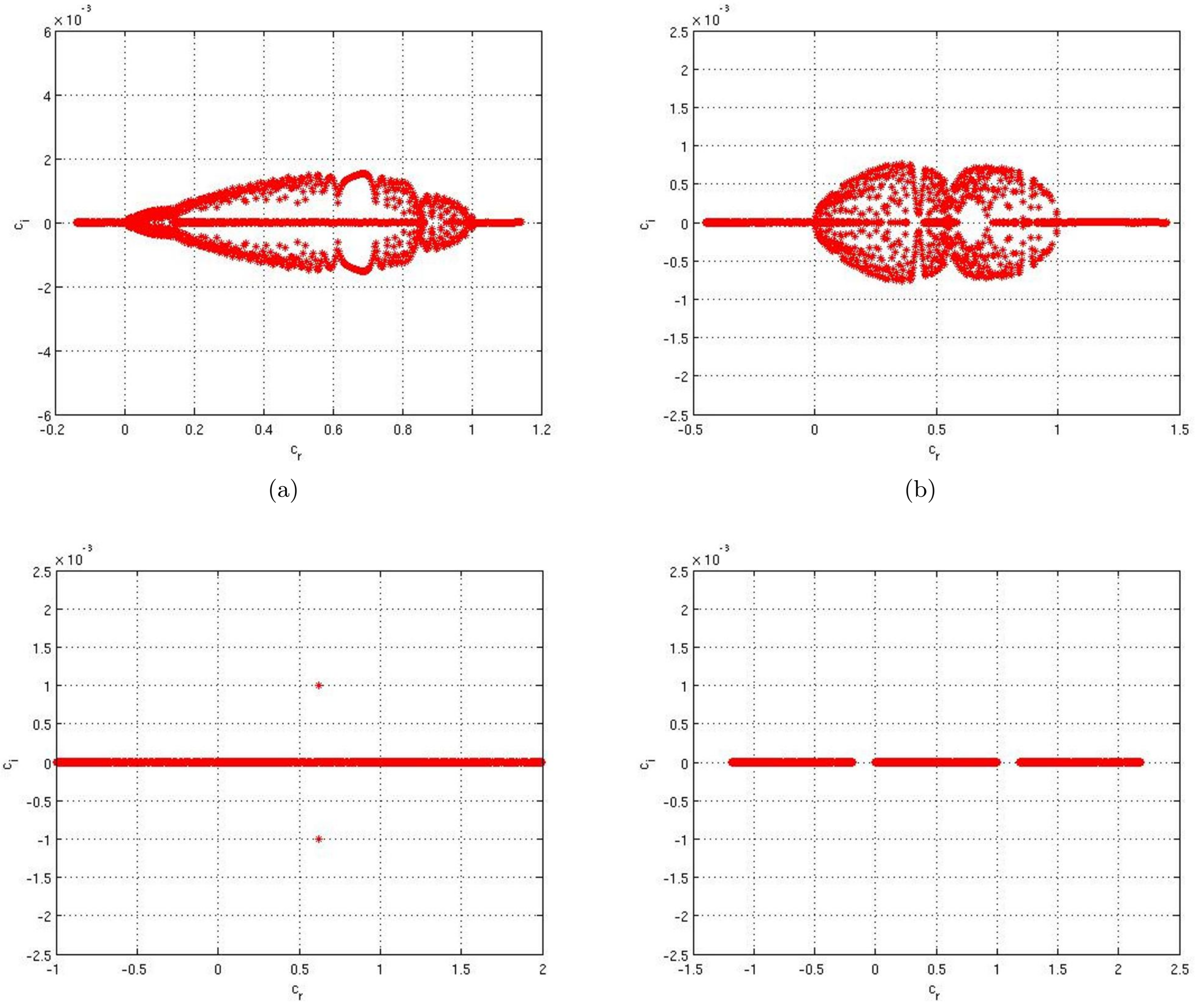

(a) (b)

(c) (d)

Figure 2.4: Elastic Couette flow spectrum with ‘N (=600)’ fixed. (a) E=0.01 (b) E=0.1 (c) E=0.5 (d) E=0.7

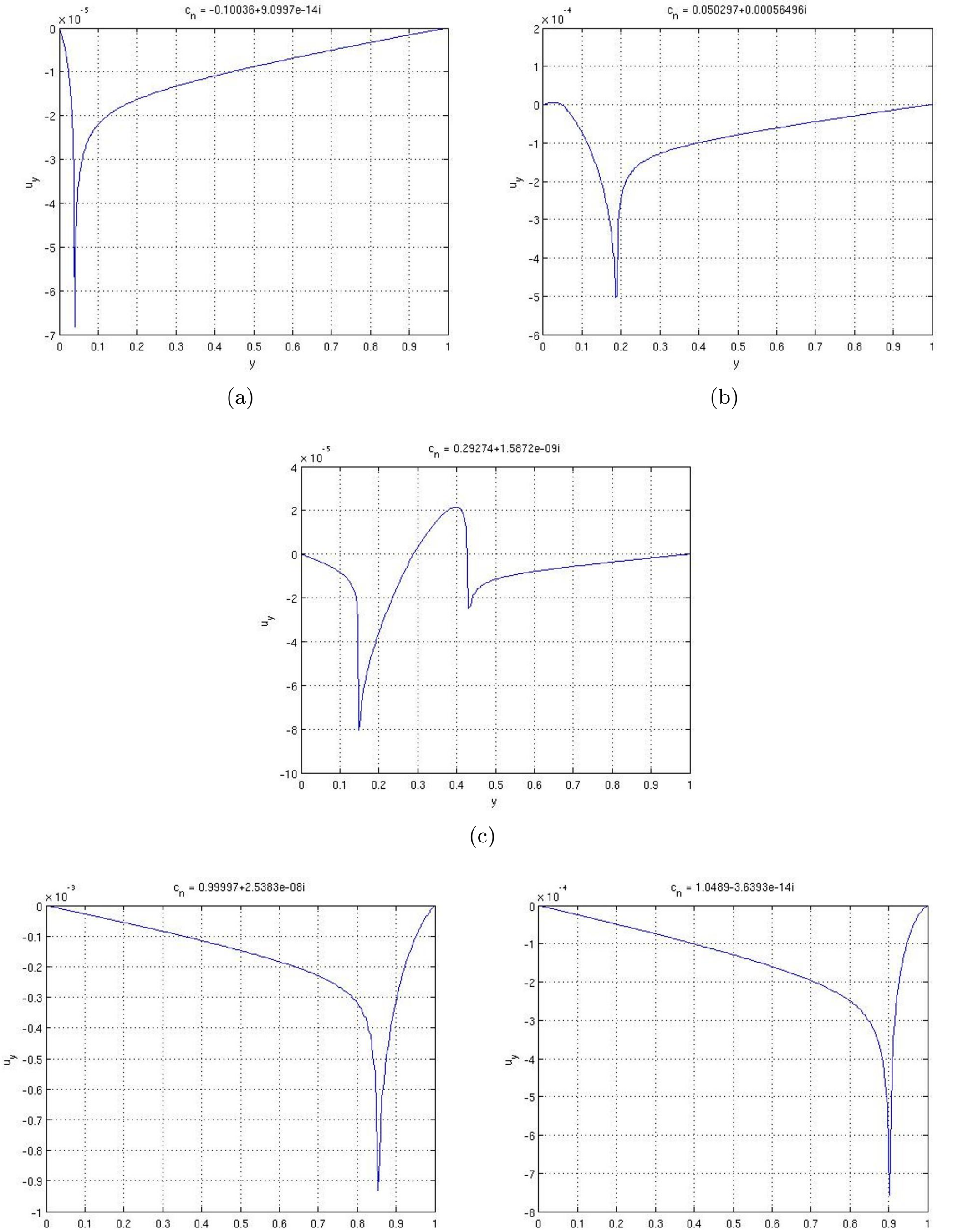

(a) (b)

(c)

(d) (e)

Figure 2.5: Eigenfunctions over complete spectrum.(a) An $FSWS$ eigenfunction (b) A superposition of the $FSWS$ and the Doppler eigenfunctions (c) A superposition of the $FSWS$, Doppler, and the $SSWS$ eigenfunctions (d) A superposition of the $SSWS$ and the Doppler eigenfunctions (e) An $SSWS$ eigenfunction

to distinct regions where two spectra overlap. Based on the theoretical estimates, mutual overlaps first disappear for $E = 0.5$, in which case the three spectra are end-to-end contiguous (the $FSWS$ spectrum from -1 to 0; the Doppler spectrum from 0 to 1; the $SSWS$ spectrum from 1 to 2). The travelling-wave singularities lie just at the edges of the domain, and accordingly, there is no ballooning. For greater values of E, the two travelling-wave spectra move farther away, and completely out of the physical domain (0 1); the Doppler spectrum alone remains in the physical domain, the associated singularity being too weak to lead to ballooning.

A quantitative comparison of the numerical eigenfunctions with the analytical ones, for instance those given by (2.49)-(2.50) and (2.51)-(2.52), is not possible. This is because, unlike the eigenvalue limits derived earlier, a comparison between the eigenfunctions would only be valid for sufficiently small $E\,((2E)^{\frac{1}{2}} \ll 1$, to be precise) when the matched asymptotic expansions approach is justified. For small E, however, the $SSWS$ and $FSWS$ intervals have a strong overlap $(y_c\,\epsilon\,[(2E)^{\frac{1}{2}}, 1-(2E)^{\frac{1}{2}}])$, and the spectral method is only expected to give some superposition of the multiple (three) travelling-wave CS-modes corresponding to any y_c in this interval. Any comparison would therefore require the inclusion of a pair of superposition parameters combining the Doppler, $FSWS$ and $SSWS$ eigenfunctions - a tedious exercise. An examination of the numerical eigenfunctions below, for finite E, is qualitative, being restricted to the identification of the travelling wave singularities; these appear as sharp peaks at the locations $y = y_c \pm (2E)^{\frac{1}{2}}$ in the numerical plots. Figure (2.5) shows the different forms taken by the inviscid elastic eigenfunctions for $E = 0.01$ and $N = 300$. For the travelling-wave eigenfunctions in the peripheral parts of the spectrum, only one of the singularities $(\mathrm{y{=}c}\pm\sqrt{2E})$ lies in the physical domain.

Chapter 3

Elastic Rankine Vortex

3.1 Introduction

Having studied explicitly the elastic continuous spectra of plane Couette flow in the last chapter, we now turn our attention to its cylindrical flow analogue: the Rankine vortex column. The Rankine vortex is the simplest of the available canonical models for vortices, and serves as a useful starting point for more realistic vorticity profiles. It consists of a cylindrical core of rigidly rotating fluid, of a fixed radius, surrounded by an irrotational exterior. An important advantage of this configuration is that it is inertially stable. As shown recently, the Rankine vortex only supports neutrally stable discrete and continuous spectrum modes, a combination of which may at best lead to algebraic growth for short times (Roy & Subramanian (2014*a*)). Note that the presence of discrete modes for the Rankine vortex (the so-called Kelvin modes) is in contrast to Couette flow (and other non-inflectional shearing flows in general) which supports a purely continuous spectrum.

The present chapter is organized as follows. In section (3.2), starting from the equations of motion and the Oldroyd-B constitutive relation, we derive the governing linearized equations for small-amplitude perturbations at finite De and Re. As a prelude to the material in section (3.4), we discuss the continuous spectra of this system of equations in 3.2.1. Next, in section (3.3) we derive the elastic Rayleigh equation in plane-polar coordinates that governs the stability of a base-state vortical flow to infinitesimal wave-like perturbations with a zero axial wavenumber in the limit $Re, De \to \infty$ with E finite. In sections 3.4.1 and 3.4.2, we examine the spectral characteristics of the elastic Rayleigh equation equation in more detail by constructing the CS-spectrum eigenfunctions using a matched asymptotic expansions approach. In section 3.4.3 we construct the perturbation vorticity, to $O(\sqrt{E})$, showing that the vorticity field, similar to the elastic Couette flow case, must be interpreted in the sense of a generalized function (a principle-finite-part interpretation). We conclude our analysis with the construction of a composite or uniformly valid solution in section 3.4.4. Finally, in section (3.5), we summarize the main results with a discussion of future lines of research.

3.2 Problem formulation

The general system of equations governing the motion of an Oldroyd-B fluid was given by (1.3)-(1.5) in chapter 1. In this chapter, we are interested in studying two-dimensional disturbances (with zero axial wavenumber) to the base-state azimuthal flow of an Oldroyd-B fluid. Let us consider $\mathbf{v} = \overline{\mathbf{u}} + \mathbf{u}, \mathbf{A} = \overline{\mathbf{A}} + \mathbf{a}$, where the overbar quantities represent the unperturbed axisymmetric base state. For an axisymmetric swirling flow, we have, $\overline{\mathbf{u}} = (0, \Omega r, 0)$, with $\Omega \equiv \Omega(r)$, and the base-state stresses being given as:

$$\overline{\mathbf{A}}(r) = \begin{bmatrix} 1 & r\Omega'\tau \\ r\Omega'\tau & 1 + 2(r\Omega'\tau)^2 \end{bmatrix} \tag{3.1}$$

in a cylindrical coordinate system where $'$ denotes a derivative w.r.t r. Note that the base-state hoop stress component($A_{\theta\theta}$), on account of the quadratic scaling with the shear rate, becomes dominant for large shear rates (r$\Omega'\tau \gg$1) except when $\Omega' = 0$ which corresponds to the trivial case of solid-body rotation. For the present analysis, we consider the Rankine vortex profile for which $\Omega(r) = \Omega_0$ for r $<$ a (the rigidly rotating core) and $\Omega(r) = \Omega_0(a/r)^2$ for r $\gg$ a. The governing equation for the perturbation velocity field is (Reddy *et al.* (2015)):

$$\frac{\partial \mathbf{u}}{\partial t} + \Omega \frac{\partial \mathbf{u}}{\partial \theta} + \mathbf{u}.\nabla\overline{\mathbf{u}} = -\nabla\left(\frac{p}{\rho}\right) + \nu\nabla^2\mathbf{u} + \frac{G}{\rho}\nabla.\mathbf{a}. \tag{3.2}$$

For the two-dimensional perturbations under consideration, $\mathbf{u} \equiv (u_r, u_\theta)$, the equations governing the perturbations to the elastic stresses are given by:

$$\left(\frac{\partial}{\partial t} + \Omega\frac{\partial}{\partial \theta} + \frac{1}{\tau}\right) a_{rr} - 2\left\{\overline{A}_{rr}\frac{\partial u_r}{\partial r} + \frac{\overline{A}_{r\theta}}{r}\frac{\partial u_r}{\partial \theta}\right\} = 0, \tag{3.3}$$

$$\begin{aligned} &\left(\frac{\partial}{\partial t} + \Omega\frac{\partial}{\partial \theta} + \frac{1}{\tau}\right) a_{r\theta} + \left\{\overline{A}'_{r\theta}u_r - \overline{A}_{r\theta}\left(\frac{\partial u_r}{\partial r} + \frac{u_r}{r}\right) - \frac{\overline{A}_{\theta\theta}}{r}\frac{\partial u_r}{\partial \theta}\right\} + \\ &\left\{\overline{A}_{rr}\left(\frac{u_\theta}{r} - \frac{\partial u_\theta}{\partial r}\right) - \frac{\overline{A}_{r\theta}}{r}\frac{\partial u_\theta}{\partial \theta}\right\} - r\Omega' a_{rr} = 0, \end{aligned} \tag{3.4}$$

$$\begin{aligned} &\left(\frac{\partial}{\partial t} + \Omega\frac{\partial}{\partial \theta} + \frac{1}{\tau}\right) a_{\theta\theta} - 2\left\{\overline{A}_{r\theta}\left(\frac{\partial u_\theta}{\partial r} - \frac{u_\theta}{r}\right) + \frac{\overline{A}_{\theta\theta}}{r}\frac{\partial u_\theta}{\partial \theta}\right\} + \\ &\left(\overline{A}'_{\theta\theta} - \frac{2\overline{A}_{\theta\theta}}{r}\right) u_r - 2r\Omega' a_{r\theta} = 0. \end{aligned} \tag{3.5}$$

On scaling lengths with the vortex core radius a, time with the turnover time based on the core angular frequency Ω_0^{-1}, and assuming a normal mode form, $f = \hat{f}(r)e^{i(m\theta-\omega t)}$, for the various perturbation fields, we have the following equations governing the r-dependent perturbation amplitudes:

$$\Sigma r\mathscr{L}(r\hat{u}_r) + mrDZ\hat{u}_r = \frac{i}{\text{Re}} r\mathscr{L}^2(r\hat{u}_r) - \frac{im}{\text{Ma}_e^2}\left[mD^*\hat{N}_1 + iDD^*(r\hat{a}_{r\theta}) + \frac{im^2}{r}\hat{a}_{r\theta}\right], \tag{3.6}$$

$$\Sigma_2\hat{a}_{rr} = 2i\left\{\overline{A}_{rr}D + \frac{im\overline{A}_{r\theta}}{r}\right\}\hat{u}_r, \tag{3.7}$$

$$\Sigma_2\hat{a}_{r\theta} = -\frac{r\overline{A}_{rr}}{m}DD^*\hat{u}_r - \left\{\frac{m}{r}\overline{A}_{\theta\theta} + i\overline{A}'_{r\theta}\right\}\hat{u}_r + i\hat{a}_{rr}r\Omega', \tag{3.8}$$

$$\Sigma_2\hat{a}_{\theta\theta} = -\frac{2r\overline{A}_{r\theta}}{m}DD^*\hat{u}_r - i\left\{\overline{A}'_{\theta\theta} + 2\overline{A}_{\theta\theta}D\right\}\hat{u}_r + 2i\hat{a}_{r\theta}r\Omega', \tag{3.9}$$

where $D \equiv \dfrac{d}{dr}$, $D^* \equiv \dfrac{d}{dr} + \dfrac{1}{r}$, $\Sigma = \omega - m\Omega$ and $\Sigma_2 = \omega - m\Omega + \dfrac{i}{\text{De}}$, and $\overline{\mathbf{A}}$ denotes the non-dimensional polymeric base-state stresses given by (3.1) above. Here, $DZ = r\Omega'' + 3\Omega'$ is the the base-state vorticity gradient and $\hat{N}_1 = \hat{a}_{\theta\theta} - \hat{a}_{rr}$ is the perturbation to the first normal stress difference. For the Rankine vortex, the base-state vorticity (Z) and vorticity gradient (DZ) are $Z(r) = 2\Omega_0 H(a-r)$ and $DZ(r) = -2\Omega_0\delta(r-a)$, $H(z)$ and $\delta(z)$ being the Heaviside and Dirac delta functions, respectively. Here, we have used the relation $\hat{w}_z = (i/m)\mathscr{L}(r\hat{u}_r)$ between the axial vorticity and radial vorticity perturbations for zero axial wave number with $\mathscr{L} = DD^* - (m^2-1)/r^2$ (Roy & Subramanian (2014*a*)). The non-dimensional parameters that appear in (3.6)-(3.9) are the Deborah number $De = \Omega_0\tau$ which is the ratio of the relaxation to the flow time scale, the Reynolds number $Re = \Omega_0 a^2/\nu_t$ which is the ratio of the viscous to the inertial time scale, and the elastic 'Mach' number $Ma_e = \Omega_0 a/c_{\text{elas}}$ which is the ratio of the flow velocity scale to $c_{\text{elas}} = \sqrt{G/\rho}$, the shear wave speed in a quiescent elastic medium. Note that in the limit $\beta \to 1$, $Ma_e \to \infty$, so that only the first term on the RHS in (3.6) survives, giving the Orr-Sommerfeld equation in cylindrical coordinates. Here onwards, we will drop $\hat{(.)}$ to denote perturbation quantities.

3.2.1 The Continuous spectrum for finite Re and De

The above system of equations (3.6)-(3.9) may be combined into a single fourth-order differential equation governing $\hat{u}_r$, the cylindrical analog of the viscoelastic Orr-Sommerfeld equation obtained in chapter 2. Apart from discrete modes, for any finite De and Re, the system (3.6)-(3.9), similar to the case of plane parallel shear flows, possesses a pair of continuous spectra (see chapter[2]). The latter are given by $r \epsilon r_c$ with r_c defined by:

$$\Sigma_2(r_c) = 0, \tag{3.10}$$

$$\Sigma_2(r_c) + i\mathrm{Re}/\mathrm{Ma}_e^2 = 0, \tag{3.11}$$

where $\Sigma_2(r)$ is as defined above (Renardy & Renardy (1986); Wilson *et al.* (1999); Kupferman (2005)). As discussed in chapter 2, the GL spectrum, defined by (3.10), continues to exist for finite Re even for the azimuthal shearing flow considered here. This is due to the assumed local nature of the polymeric stress field in almost all constitutive equations in polymer rheology (Bird *et al.* (1987)). This in turn arises from the neglect of the centre-of-mass diffusion of polymer molecules, so the resulting polymeric fluid is a simple fluid in the continuum mechanics parlance (Coleman & Noll (1961)). As a result, not withstanding the coupling due to the perturbation flow driven by the stress gradient (via the equations of motion), the polymeric stress along a given streamline develops in a manner independent of the neighboring ones. This local evolution is exemplified by the existence of singular divergence-free eigenfunctions for the stress field first derived by Kupferman (2005). The evolution of the polymeric stress field in the absence of center-of-mass diffusion is, in fact, similar to that of the vorticity field in the inviscid limit, and both cases, in principle, allow for arbitrarily large gradients across streamlines (Roy (2012); Roy & Subramanian (2014*b*)). Based on this analogy, one expects CS-modes with singularities in the polymeric stress fields. Similar to the parallel flow case, the singular GL-eigenfunctions, in addition to being convected with the flow velocity at $\mathrm{r} = \mathrm{r}_c$, decay at a rate De^{-1} due to relaxation, asymptoting to neutral stability for $De \to \infty$. Further, similar to the plane parallel case, the GL spectrum in cylindrical coordinates is characterized by the Frobenius exponents 0, 1, 3 and 4, the streamline curvature being negligible on the length scales defining the validity of the local Frobenius analysis. A finite solvent viscosity gives rise to the viscous continuous spectrum (Wilson *et al.* (1999)). The Frobenius exponents characterizing this spectrum in genreal involve fractional parts - 0,1, 2 and 3 -$2/\beta$, and hence similar to the case of plane Couette flow in chapter 2, the CS-eigenfunctions requires the principal-finite-part-interpretation. Having derived the general linear equation governing small-amplitude perturbations, in the next section we look at the regime of interest Re$\to \infty$ and De$\to \infty$ which involves neglecting all terms corresponding to microstructural relaxation. In this limit, there will be a reduction in the order of the governing equation from four to two.

3.3 Elastic Rayleigh Equation (Re→ ∞ and De→ ∞)

The stability investigations in the above mentioned limit ($Re \to \infty$, $De \to \infty$) have been carried out by Azaiez & Homsy (1994), and more recently by Renardy (2008) and Kaffel & Renardy (2010). Azaiez & Homsy (1994) studied the role of elasticity on the linear stability of an inertially unstable mixing layer and the spectrum showed that fluid elasticity has stabilizing effects. Rallison & Hinch (1995) analyzed the stability of a submerged jet (both planar and axisymmetric), another flow configuration susceptible to inertial instabilities. Once again, elasticity for the most part acts to stabilize the unstable inertial modes, but the authors also discovered a novel instability caused by elasticity. This instability arises from a resonant interaction of elastic shear waves, and the waves in turn arise from a balance of inertia and elasticity. If one defines an elasticity parameter, $E = De^2/Ma_e^2 = De/Re = \mu_p\tau/(\rho a^2)$, then the non-dimensional speed of propagation of a shear wave relative to the local flow is $O(\sqrt{\mathrm{E}})$. The ambient shear associated with the jet profile allows for a forward traveling shear wave, close to the jet boundary, to resonate with a backward travelling shear wave located at an $O(\sqrt{\mathrm{E}})$ distance in the interior, and this resonance leads to the instability. Unlike these earlier efforts, whose focus was solely on the discrete modes, the present effort is focussed on the elastic continuous spectrum which also includes singular eigenfunctions representative of the shear waves above.

Before examining the elastic continuous spectra, we first consider the elastic Rayleigh equation in more detail. The single equation for u_r governing the perturbations, in the limit $Re, De \to \infty$, reduces to:

$$\Sigma\left(r^2D^2u_r + 3rDu_r - (m^2-1)u_r\right) + mrDZu_r =$$
$$2m^2\mathrm{E}\Big[2D^*\left\{\frac{r\Omega'}{\Sigma}\left(\frac{mr\Omega'^2}{\Sigma} + r\Omega'D^* + r\Omega''\right)u_r\right\} - \left(rD^2 + 3D + \frac{m^2}{r}\right)\left(\frac{r\Omega'^2}{\Sigma}\right)u_r\Big] \quad (3.12)$$

or equivalently,

$$\Sigma^3\left[\Sigma r\left(r^2D^2u_r + 3rDu_r - (m^2-1)u_r\right) + mrDZu_r\right] = 2m^2\mathrm{E}\Omega'\Big[\Sigma^2\Big\{r^2\Omega'D^2u_r + r(r\Omega'' + DZ)Du_r$$
$$-(m^2-1)\Omega'u_r\Big\} + mr\Omega'\Sigma\Big\{2r\Omega'Du_r + 3(DZ - 2\Omega')u_r\Big\} + 2m^2r^2\Omega'^3u_r\Big]. \quad (3.13)$$

The above equation is the elastic equivalent of the Rayleigh equation for swirling flows (refer to section 15.3 in Drazin & Reid (1981)). The terms proportional to E in (3.12) and (3.13) denote the contributions due to elasticity. Thus, the original fourth order ODE equation resulting from

(3.6)-(3.9) reduces to a second-order ODE in the limit $De \rightarrow \infty$, E fixed, implying that the neglect of relaxation is a singular limit.

It is worth noting here that for typical inertio-viscoelastic flows, E is the parameter governing competing effects of inertia and viscoelasticity only for small but finite De when relaxation effects are dominant and the fluid rheology is describable in terms of a retarded motion expansion (see, for instance, Dabade & Subramanian (2015)). For large De, relaxation is unimportant with the dynamics in the polymeric fluid at finite Re being governed by elastic shear waves damped due to the solvent viscosity alone (Gorodtsov & Leonov (1967)). In this limit, Ma_e becomes the governing parameter (Joseph (2007)). It is thus a little surprising that in the limit of large De considered here, E rather than Ma_e turns out to be relevant for (3.14), suggesting the continued importance of relaxation (τ). However, E in (3.14) is more appropriately interpreted in terms of a viscoelastic Mach number where the sonic speed corresponds to shear waves propagating in a pre-stressed elastic medium. The base-state stress level is $\bar{A}_{\theta\theta} \sim O(De^2)$ as given earlier, and the shear wave speed relevant to the perturbation dynamics is given by $\sqrt{G\bar{A}_{\theta\theta}/\rho} \sim De\sqrt{G/\rho}$. The relevant Mach number is $O(De).O(\sqrt{G/\rho}/\Omega_0 a) \sim (De/Re)^{1/2} \sim E^{1/2}$. Thus, the rather paradoxical dependence on E, and thence on the relaxation time, occurs via the shear wave speed being dependent on the base-state hoop stress which directly depends on τ. This is much like the classical viscous stability analyses of Newtonian fluids, where viscosity plays a crucial role in setting up the base-state velocity profile, while playing a (relatively) sub-dominant role in the dynamics of perturbations at large Re.

The elastic Rayleigh equation may be written in a more compact form in terms of the radial displacement, $\xi \equiv iu_r/\Sigma$, first identified by Rallison & Hinch (1995) in the context of plane parallel shearing flows, and given by:

$$D\left[r^3 P D\xi\right] = r(m^2-1)P\xi \tag{3.14}$$

$$\text{where,} \qquad P = \Sigma^2 - 2m^2\mathrm{E}\Omega'^2, \quad \Sigma = \omega - m\Omega \quad \text{and} \quad \xi = \frac{iu_r}{\Sigma} \quad \text{(the radial displacement)}$$

From (3.14), one may easily construct the following modified version of Howard semi-circle theorem (Howard & Gupta (1962)) for swirling flows:

$$\left(\omega_r - \frac{m(\Omega_{max}+\Omega_{min})}{2}\right)^2 + \omega_i^2 \;\; \leq \;\; m^2\left(\frac{\Omega_{max}-\Omega_{min}}{2}\right)^2 - 2m^2E\Omega'^2_{min}. \tag{3.15}$$

One can see that the role of elasticity is to shrink the inviscid semi-circle of instability, implying a relative stabilization. The analog of (3.14) has been used by Rallison & Hinch (1995) in their study of elastic instabilities in jets. Absolute stability results when the semi-circle radius decreases to zero, and this happens at a finite E provided Ω'_{min} is non-zero.

From (3.14), it is seen that the elastic Rayleigh equation has a pair of singular points given by $P(r_c) = 0$. In terms of ω, the singularities correspond to $\omega = m\Omega \pm m\Omega'\sqrt{2\mathrm{E}}$. Physically, these singularities correspond to fore- and aft- traveling elastic shear waves (relative to the local flow at r). Thus, for the elastic Rayleigh equation, there exist a pair of continuous spectra associated with fore- and aft-travelling elastic shear waves in the azimuthal direction that owe their origin entirely to elasticity. Unlike the finite De continuous spectra discussed above, these inviscid travelling-wave spectra arise due to a balance of the inertial and elastic terms, and must disappear for any finite De. Thus, in the presence of any amount of relaxation, the travelling-wave CS-modes are no longer true eigenfunctions, and must instead be expressible in terms of a superposition of finite De discrete modes. Aside from the obvious reduction in the order of the equation, this again highlights the singular relation between the spectrum of the elastic Rayleigh equation discussed below and the finite De spectrum. The effects of a weak relaxation are analyzed in chapter 4. The elastic Rayleigh operator also supports a third continuous spectrum ranging over the base-state interval of angular velocities, which is the original inviscid continuous spectrum (Case (1960); Roy & Subramanian (2014*a*)) modified by elasticity. This spectrum arises despite the critical level ($r = r_c$) being an ordinary point of (3.14); the exponents for the radial displacement field being 0 and 1 (those for the radial velocity are 1 and 2). This arises from considering the special case of the Rankine vortex (or plane Couette flow), and is also the case for the original inviscid Rayleigh equation. In this case, the point $r = r_c$ for the Rankine case must be regarded as the limiting case of a general vorticity profile where one of the solutions at the critical level is indeed logarithmically singular, and leads to a continuous spectrum. In what follows, we analyze in detail the pair of continuous spectra associated with the travelling wave singularities.

3.4 Boundary layer analysis of the elastic Rayleigh equation

In this section, we solve for the CS-spectrum eigenfunction via a matched asymptotics expansions approach for small E. As noted in chapter 2, the elastic Rayleigh equation, being a member of the confluent Heun class, is not amenable to any analysis for arbitrary E. An analysis at small E yields significant insight owing to the singular effect of elasticity. The original inviscid eigenfunctions of the Rankine vortex are non-trivially altered in an $O(E^{\frac{1}{2}})$ elastic boundary layer around $r = r_c$.

3.4.1 The outer solutions

To begin with, we summarize briefly the inviscid 2D CS-spectrum of the Rankine vortex for $E = 0$ as found by Roy & Subramanian (2014*a*), and referred to as the Λ_1-family therein. For an azimuthal wavenumber m, the 2D CS-modes span the angular frequency range (0, mΩ_0), and have a twin-vortex-sheet structure. The vortex sheets are cylindrical, being threaded by axial lines, with one sheet located at the edge of the core and the other at the critical radius in the irrotational exterior. A given CS-mode rotates with the base-angular velocity corresponding to the critical radius. Therefore, the radial velocity and vorticity eigenfunctions are of the form $\big[u_r(r; r_c), \omega_z(r; r_c)\big] = \big[\hat{u}_r(r; r_c); \hat{\omega}_z(r; r_c)\big]e^{i(m\theta-\omega t)}$ with $\omega = m\Omega(r_c)$, $r_c = (m/\omega)^{1/2}$ and

$$\begin{aligned}
\hat{u}_r(r; r_c) &= dr^{m-1} \qquad r < 1, && (3.16)\\
&= ar^{m-1} + b\frac{1}{r^{m+1}} \qquad 1 < r < r_c, && (3.17)\\
&= \frac{1}{r_c}\frac{1}{r^{m+1}} \qquad r > r_c, && (3.18)\\
\hat{\omega}_z(r; r_c) &= \Big[\frac{2id}{\omega - m}\delta(r-1) - A(r_c)\delta(r-r_c)\Big], && (3.19)
\end{aligned}$$

where

$$\begin{aligned}
d &= \frac{1}{r_c} + \frac{iA(r_c)}{2}\Big[r^{m+1} - \frac{1}{r^{m-1}}\Big], && (3.20)\\
a &= -\frac{iA(r_c)}{2}\frac{1}{r^{m-1}}, && (3.21)\\
b &= \frac{1}{r_c} + \frac{iA(r_c)}{2}r^{m+1}, && (3.22)\\
A(r_c) &= \frac{(2i/r_c)\big[(m-1)-\omega\big]}{(1/r_c^{m-1}) + \big[(m-1)-\omega\big]r_c^{m+1}}, && (3.23)
\end{aligned}$$

The radial velocity eigenfunction itself is continuous at $r = r_c$, but the discontinuity in slope at both $r = 1$ and $r = r_c$ corresponds to delta-function (vortex-sheet) contributions in the perturbation axial vorticity field. The first delta function is an artifact of the kink in the base-state (Rankine) profile, and consideration of a smooth velocity leads to a continous eigenfunction. It is thus the amplitude of the second vortex sheet, $A(r_c)$, that is of interest and that characterizes the 2D CS-spectrum. Note that $A(r_c)$ equals zero when $\omega = (m-1)$, which corresponds to the regular Kelvin mode with a critical radius given by $r_{ck} = (\frac{m}{m-1})^{1/2}$. There is a direct analogy between the 2D CS-spectra of plane Couette flow as found by Case (1960) and that of the Rankine vortex summarized above. In both cases, the vorticity eigenfunctions are vortex-sheets convected with the base-state flow - a single plane vortex sheet for Couette flow and a pair of cylindrical sheets for the Rankine vortex. The crucial difference is the additional presence of the Kelvin mode above in the latter case. While the inviscid spectrum for plane Couette flow (and other non-inflectional profiles) is purely continuous with the amplitude of the vortex-sheet remaining non-zero over the entire range of wave speeds, there exists a unique angular frequency, for a given m, for which the vortex-sheet amplitude is zero for the case of the Rankine vortex. The Kelvin mode, together with the 2D CS-modes provide a complete basis for an arbitrary axial vorticity field in two dimensions (Roy & Subramanian (2014*a*)).

For small but finite E, we examine the solutions of (3.14) separately in the outer region where $r - r_c \sim O(1)$, and in the inner region where $r - r_c \sim O(\sqrt{E})$, before matching them to determine the unknown coefficients in the respective domains. We assume the critical radius, r_c, to be such that the elastic boundary layer lies an $O(1)$ distance away from the edge of the core $(r = 1)$. The solutions in the outer regions, at leading order, are thus identical to those given in (3.16)-(3.18) except that (3.17) and (3.18) are not valid right until r_c. Likewise, apart from the core contribution (the term proportional to $\delta(r-1)$ in (3.19), the vorticity field is localized in the elastic boundary layer around r_c, although no longer a delta function at this location. Thus, (3.17) is now valid in the range $r > 1$, $(r_c - r) \gg O(E^{1/2})$ while (3.18) is now valid in the range $(r - r_c) \gg O(E^{1/2})$. Note that since $P = \Sigma^2 - 2m^2 \mathrm{E}\Omega'^2$ in (3.14), the direct effect of elasticity enters the outer regions only at $O(E)$. At $O(E^{\frac{1}{2}})$, the outer solutions still satisfy the inviscid Rayleigh equation, and the effects of elasticity only enter via matching to the far-field forms of the elastic boundary layer solution. For purposes of matching below, it is convenient to normalize the perturbation in the core region, so that $\hat{u}_r(r;r_c) = r^{m-1}$ for $r < 1$, instead of (3.16) (this being valid to all orders in E). As a result, instead of (3.17) and (3.18), we have:

$$\hat{u}_{r1}(r;r_c) = a_0^- r^{m-1} + \frac{(1-a_0^-)}{r^{m+1}} + E^{1/2} a_1^- (r^{m-1} - \frac{1}{r^{m+1}}) + O(E) \quad r > 1, r_c - r \gg O(E^{1/2}) \tag{3.24}$$

$$\hat{u}_{r2}(r;r_c) = \frac{b_0^+ + E^{1/2} b_1^+}{r^{m+1}} + O(E) \quad r - r_c \gg O(E^{1/2}), \tag{3.25}$$

for the irrotational radial velocity perturbation outside the core and outside the elastic boundary layer. Here, we used superscripts ± with constants representing the regions $(r - r_c) \gg O(E^{1/2})$ and $(r_c - r) \gg O(E^{1/2})$ respectively. The choice of constants in (3.24) and (3.25) reflects consistency with the normalized core perturbation at $r = 1$. Since one is looking for elastic generalizations of the Λ_1 CS-modes, we also impose continuity of the radial velocity for $r \to r_c$, as seen from the outer region. This implies $a_0^- r_c^{m-1} + \frac{(1-a_0^-)}{r^{m+1}} = \frac{(b_1^-)}{r_c^{m+1}} = \hat{u}_r(r; r_c)$, which also leads to the relation between the two constants involved: $b_0^+ = a_0^+(r_c^{2m} - 1)$.

It may be shown that a balance between the inertial and elastic terms occurs at leading order when $(r - r_c) \sim O(E^{1/2})$, and one therefore defines the elastic boundary layer variable (see Figure(3.1)):

$$\eta = \frac{r - r_c}{\sqrt{2\mathrm{E}}} \tag{3.26}$$

We use the expansion,

$$\Sigma(r_c) = 0 \Rightarrow \Sigma \approx -m\Omega_c^{-1}(r - r_c) - m\Omega_c''\frac{(r - r_c)^2}{2} \cdots , \tag{3.27}$$

$$\approx \quad -m\Omega_c'\sqrt{2E}\Big\{\eta + \frac{\Omega_c''}{\Omega_c'}\sqrt{\frac{E}{2}}\eta^2\Big\} \cdots \tag{3.28}$$

By definition the relation between the radial velocity and displacement is give by:

$$u_r(r) = \tilde{u}_r(\eta) \quad \text{and} \quad \xi(r) = \frac{\tilde{\xi}(\eta)}{\sqrt{2E}}, \quad \text{then} \tag{3.29}$$

On using (3.27), the above relation takes the form in the boundary layer, to O(E):

$$\begin{aligned} u_r(r) &= i\Sigma\xi(r) \qquad (3.30) \\ \tilde{u}_r(\eta) &= i\Sigma\frac{\tilde{\xi}(\eta)}{\sqrt{2E}} \approx -im\Omega_c'\eta\Big\{1 + \frac{\Omega_c''}{\Omega_c'}\sqrt{\frac{E}{2}}\eta\Big\}\tilde{\xi}(\eta) \end{aligned}$$

Now consider the expansion,

$$\tilde{\xi}(\eta) = \tilde{\xi}^{(0)}(\eta) + \sqrt{E}\tilde{\xi}^{(1)}(\eta) + \cdots \tag{3.31}$$

$$\tilde{u_r}(\eta) = \tilde{u}_r^{(0)}(\eta) + \sqrt{E}\tilde{u}_r^{(0)}(\eta) \cdots \tag{3.32}$$

on substituting in the above relation, we have,

$$\tilde{u}_r^{(0)}(\eta) = -im\Omega_c'\eta\tilde{\xi}^{(0)}(\eta) \tag{3.33}$$

$$\tilde{u}_r^{(1)}(\eta) = -im\Omega_c'\eta\Big[\tilde{\xi}^{(1)}(\eta) + \frac{\eta}{\sqrt{2}}\frac{\Omega_c''}{\Omega_c'}\tilde{\xi}^{(0)}(\eta)\Big] \tag{3.34}$$

On rewriting the elastic Rayleigh equation (ERE) in terms of newly defined boundary layer co-ordinates, we have,

$$\frac{1}{2E}\frac{d}{d\eta}\Big[\Big\{r_c + \sqrt{2E}\eta\Big\}^3 P\frac{d\tilde{\xi}}{d\eta}\Big] = \Big\{r_c + \sqrt{2E}\eta\Big\}(m^2-1)P\tilde{\xi} \tag{3.35}$$

where

$$P = \Sigma^2 - 2m^2\mathrm{E}\Omega'^2 \tag{3.36}$$

$$\approx m^2\Omega'^2 2E\eta^2\Big\{1 + \frac{\Omega_c''}{\Omega_c'}\sqrt{2E}\eta\Big\} - 2m^2E\Omega'^2$$

$$\approx 2m^2E\Omega'^2\Big[\eta^2 - 1 + \frac{\Omega_c''}{\Omega_c'}\sqrt{2E}\eta^3\Big] \tag{3.37}$$

on substituting for P, we get

$$\frac{d}{d\eta}\Big[(1 + \frac{3\sqrt{2E}\eta}{r_c})\Big(\eta^2 - 1 + \frac{\Omega_c''}{\Omega_c'}\sqrt{2E}\eta^3\Big)\frac{d}{d\eta}\Big\{\tilde{\xi}^{(0)} + \tilde{\xi}^{(1)}\Big\}$$

$$= 2E\frac{(m^2-1)}{r_c^2}(1 + \frac{\sqrt{2E}\eta}{r_c})\Big(\eta^2 - 1 + \frac{\Omega_c''}{\Omega_c'}\sqrt{2E}\eta^3\Big)\Big\{\tilde{\xi}^{(0)} + \tilde{\xi}^{(1)}\Big\} \tag{3.38}$$

On considering terms of the same order, one obtains the following governing equations at $O(1)$ and $O(E^{\frac{1}{2}})$, respectively:

$$\frac{d}{d\eta}\Big[(\eta^2-1)\frac{d\tilde{\xi}^{(0)}}{d\eta}\Big] = 0, \tag{3.39}$$

$$\frac{d}{d\eta}\Big[(\eta^2-1)\frac{d\tilde{\xi}^{(1)}}{d\eta} + \Big\{\frac{3\sqrt{2}}{r_c}\eta(\eta^2-1) + \frac{\Omega_c''}{\Omega_c'}\sqrt{2}\eta^3 - \frac{\Omega_c''}{\Omega_c'}2\sqrt{2}\eta\Big\}\frac{d\tilde{\xi}^{(0)}}{d\eta}\Big] = 0, \tag{3.40}$$

It is worth noting that the structure of the leading order equation (3.39), is identical to (2.22) in the elastic Couette flow case (see chapter 2), and hence we expect solutions to take identical form. The solution of (3.39) is given by:

$$\tilde{\xi}^{(0)}(\eta) = A_1\eta + A_2\eta\ln\left|\frac{\eta-1}{\eta+1}\right|, \tag{3.41}$$

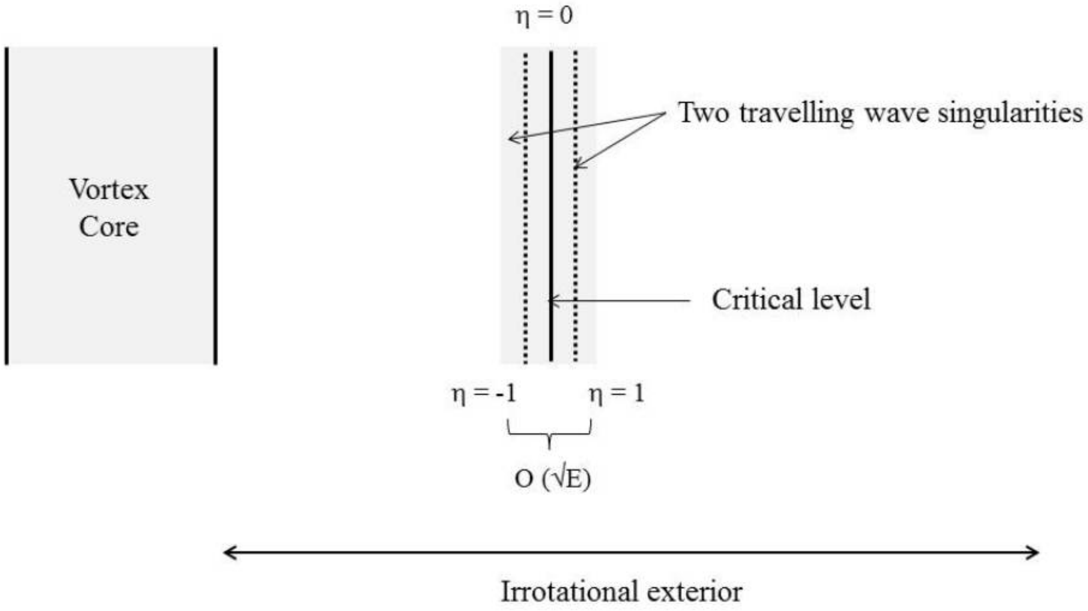

Figure 3.1: Distribution of different regions in elastic vortex

implying a radial velocity in the boundary layer of the form:

$$\tilde{u}_r^{(0)}(\eta) \quad = \quad -im\Omega_c'\eta\Big[A_1 + A_2 \ln\left|\frac{\eta-1}{\eta+1}\right|\Big], \tag{3.42}$$

at leading order. Even in the present case the values $\eta = \pm 1$ denote the locations of the travelling wave singularities where the radial velocity is logarithmically divergent. It is these singularities that divide the elastic boundary layer (EBL) into three distinct regions.

The solution forms in the individual regions may be written explicitly as:

$$\tilde{u}_{r-}^{(0)}(\eta) \quad = \quad \eta\Big[C_1^- + C_2 \ln\left|\frac{\eta-1}{\eta+1}\right|\Big] \qquad \eta < -1 \tag{3.43}$$

$$\tilde{u}_r^{(0)}(\eta) \quad = \quad \eta\Big[C_1 + C_2 \ln\frac{1-\eta}{1+\eta}\Big] \qquad -1 < \eta < 1 \tag{3.44}$$

$$\tilde{u}_{r+}^{(0)}(\eta) \quad = \quad \eta\Big[C_1^+ + C_2 \ln\frac{\eta-1}{\eta+1}\Big] \qquad \eta > 1 \tag{3.45}$$

where $C_i = -im\Omega_c' A_i$. Note that similar to the case of elastic Couette flow (see chapter 2), here we have chosen the same constant for the singular logarithmic solution in all three parts of the boundary layer. The constant C_1 in the present case is the vortex analog of the constant B_1 for plane Couette flow, and can be chosen idependently. It is this added degree of freedom which is crucial to the existence of multiple continuous spectra for finite E. Using (3.41) in (3.40), and solving, gives:

$$\tilde{\xi}_1 = A_3 + A_4 \ln\left|\frac{\eta-1}{\eta+1}\right| + \frac{i u_r(r_c)}{\sqrt{2} m \Omega'_c}\Big[\Big\{\frac{3}{r_c} + \frac{\Omega''_c}{\Omega'_c}\Big\}\ln(\eta^2-1) - \frac{\Omega''_c}{\Omega'_c}\Big(\frac{1}{\eta^2-1}\Big)\Big] \tag{3.46}$$

at the next order. Here, on using $\frac{\Omega''(r_c)}{\Omega'(r_c)} = -\frac{3}{r_c}$ for a Rankine vortex, we have:

$$\tilde{u}_{r1} = \eta\Big[C_3 + \Big\{C_4 + \frac{3C_2}{\sqrt{2} r_c}\eta\Big\}\ln\left|\frac{\eta-1}{\eta+1}\right| - \frac{3\sqrt{2}C_2}{r_c}\Big(\frac{1}{\eta^2-1}\Big)\Big] \tag{3.47}$$

for the radial velocity at $O(E^{\frac{1}{2}})$, where $C_i = -im\Omega'_c A_i$; here, as at leading order, the constant C_3 must take different values in the three parts of the elastic boundary layer. Unlike the plane Couette flow case, here one needs to go beyond the leading-order solutions in order to discriminate between the discrete and continuous spectrum modes in the original inviscid spectrum (recall that the spectrum for non-inflectional plane parallel shearing flow profiles, including plane Couette flow, is purely continuous).

3.4.2 Matching the inner (boundary layer) and outer solutions:

To determine the unknown constants C_1, $[C_2, C_2^{\pm}]$, $[C_3, C_3^{\pm}]$ and C_4, we now match the inner boundary layer (BL) solutions to the outer inviscid solutions. The matching requirement between the outer regions and those in the elastic boundary layer, is given by the following matching rule:

$$\tilde{u}^{(i)}_{r+}(\eta)|_{\eta\to\infty} \quad \Leftrightarrow \quad \hat{u}^{(i)}_{r2}(r;r_c)|_{r\to r_c^+} \tag{3.48}$$

$$\tilde{u}^{(i)}_{r-}(\eta)|_{\eta\to-\infty} \quad \Leftrightarrow \quad \hat{u}^{(i)}_{r1}(r;r_c)|_{r\to r_c^-} \tag{3.49}$$

O(1) Matching:

The far-field forms of the inner solutions are given by:

$$\tilde{u}^{(0)}_{r-}(\eta)|_{\eta\to-\infty} \quad = \quad C_1^-\eta - 2C_2^- \tag{3.50}$$

$$\tilde{u}^{(0)}_{r+}(\eta)|_{\eta\to\infty} \quad = \quad C_1^+\eta - 2C_2^+ \tag{3.51}$$

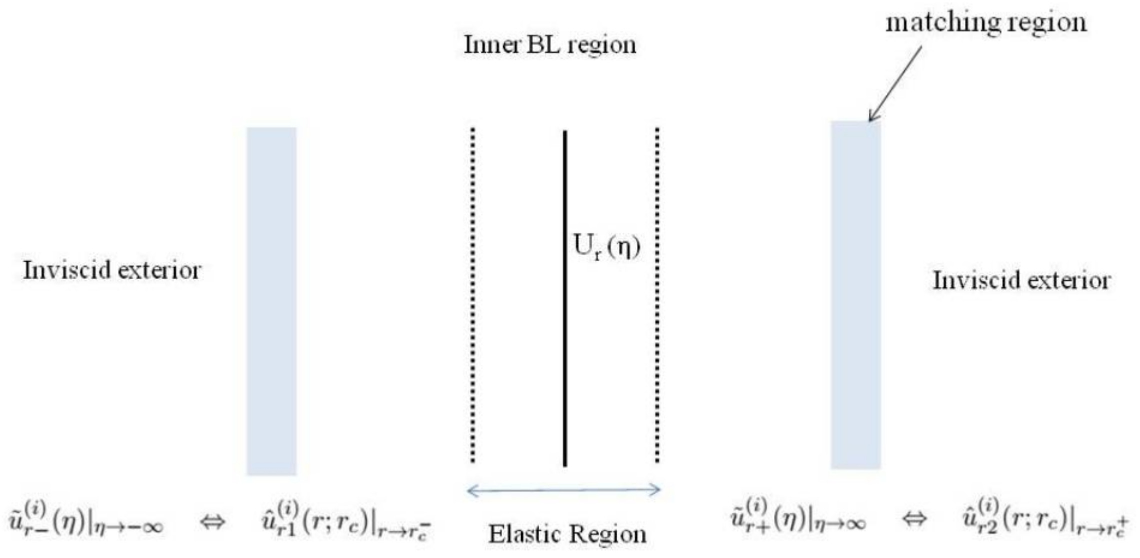
matching region
Inner BL region
$U_r(\eta)$
Inviscid exterior
Inviscid exterior
$\tilde{u}_{r-}^{(i)}(\eta)|_{\eta\to-\infty}$ ⇔ $\hat{u}_{r1}^{(i)}(r;r_c)|_{r\to r_c^-}$
Elastic Region
$\tilde{u}_{r+}^{(i)}(\eta)|_{\eta\to\infty}$ ⇔ $\hat{u}_{r2}^{(i)}(r;r_c)|_{r\to r_c^+}$

Figure 3.2: Matching inner and outer regions

The near-Field forms of the outer solutions are given by:

$$\hat{u}_{r1}^{(0)}(r;r_c) = a_0^- r^{(m-1)} + b_0^- r^{-(m+1)} \tag{3.52}$$

$$\hat{u}_{r2}^{(0)}(r;r_c) = \frac{b_0^+}{r^{(m+1)}} \tag{3.53}$$

The above solutions satisfy the boundary conditions $\hat{u}_{r1}^{(0)}(1;r_c) = 1$ (velocity field at the edge of the vortex core is assumed to be unity) and the far-field boundary condition, $\hat{u}_{r2}^{(0)}(\infty;r_c) \to 0$ (see Figure 3.2).

$$\Rightarrow \hat{u}_{r1}^{(0)}(r;r_c)|_{r\to r_c} = a_0^-(r_c{}^{(m-1)}) + (1-a_0^-)r_c{}^{-(m+1)}, \tag{3.54}$$

$$\hat{u}_{r2}^{(0)}(r;r_c)|_{r\to r_c} = \frac{b_0^+}{r_c{}^{(m+1)}} \tag{3.55}$$

On matching, one obtains the following values for the constants involved:

$$b_0^+ = \hat{u}_r(r_c;r_c)r_c^{(m+1)}, \quad C_1^\pm = 0 \tag{3.56}$$

$$a_0^- = 1 - b_0^- = -\Big[\frac{2C_2^- + r_c^{-(m+1)}}{r_c^{(m+1)} - r_c^{-(m+1)}}\Big] \quad \text{with} \quad C_2 = -\frac{\hat{u}_r(r_c;r_c)}{2} \tag{3.57}$$

Hence, all the constants at $O(1)$, except C_1, are determined. As pointed out earlier, the only difference between the 2D inviscid spectra of plane Couette flow and the Rankine vortex is the existence of a lone discrete mode - the Kelvin mode - in the latter case. In order to discriminate between the generalizations of the inviscid CS-modes and the Kelvin mode for non-zero E, one needs to carry out the matching to $O(E^{\frac{1}{2}})$. At $O(1)$, the matching process above ensures the continuity of the radial velocity across the elastic boundary layer, and it is only at $O(E^{\frac{1}{2}})$ that the two ends of the elastic boundary layer ($\eta \to \pm\infty$) sense the difference in the slopes of the outer eigenfunctions, $\hat{u}_{r1}(r;r_c)$ and $\hat{u}_{r2}(r;r_c)$, for r approaching r_c. It is precisely this jump in slope that differentiates the CS-modes from the Kelvin mode.

O($\sqrt{E}$) Matching:

The outer solutions at $O(\sqrt{E})$ are given by:

$$\hat{u}_{r1}^{(1)}(r;r_c) = a_1^- r^{(m-1)} + b_1^- r^{-(m+1)} \tag{3.58}$$

$$\hat{u}_{r2}^{(1)}(r;r_c) = \frac{b_1^+}{r^{(m+1)}} \tag{3.59}$$

The above solutions satisfy the conditions $\hat{u}_{r1}^{(1)}(1;r_c) = 0$, which gives $a_1^- = -b_1^-$. The resulting near field-forms of the outer solution at $O(E^{\frac{1}{2}})$ are given by:

$$\begin{aligned} \hat{u}_{r1}^{(1)}(r;r_c)|_{r\to r_c} &= a_1^-\left[({r_c}^{(m-1)}) + {r_c}^{-(m+1)}\right] + a_0^-(m-1)\sqrt{2}\eta({r_c}^{(m-2)}) \\ &\quad -(1-a_0^-)(m+1)\sqrt{2}\eta {r_c}^{-(m+2)} \qquad (3.60) \\ \hat{u}_{r2}^{(1)}(r;r_c)|_{r\to r_c} &= \frac{b_1^+}{{r_c}^{(m+1)}} - \frac{\sqrt{2}b_0^+(m+1)\eta}{{r_c}^{(m+2)}} \qquad (3.61) \end{aligned}$$

The $O(E^{\frac{1}{2}})$ inner solutions are given by (3.47), and on matching far-field forms of (3.47) in different regions to the near-field forms of outer solutions discussed above, we have following relations for the constants:

$$b_1^+ = b_1^- = C_4^+ = C_4^- = 0, \tag{3.62}$$

$$\begin{aligned} C_3^- &= \sqrt{2}a_0^-\left[(m-1){r_c}^{(m-2)} + (m+1){r_c}^{-(m+2)}\right] - \sqrt{2}(m+1){r_c}^{-(m+2)} - \frac{3\sqrt{2}C_2}{r_c} \\ &= -\frac{3}{\sqrt{2}r_c}\hat{u}_r(r_c;r_c) + \sqrt{2}\Big[\frac{(m-1)r_c^{2m} + (m+1)}{r_c^{m+2}}\,\frac{r_c^{m+1}\hat{u}_r(r_c;r_c) - 1}{r_c^{2m}-1} - \frac{m+1}{r_c^{m+2}}\Big] \qquad (3.63) \end{aligned}$$

$$\begin{aligned} C_3^+ &= -\frac{(m+1)\sqrt{2}}{r_c^{(m+2)}} b_0^+ + \frac{3\sqrt{2}}{r_c} C_2 \\ &= -\frac{(2m+5)}{\sqrt{2} r_c} \hat{u}_r(r; r_c), \end{aligned} \tag{3.64}$$

Having determined the constants above, the forms of the eigenfunction in the outer regions, to $O(E^{\frac{1}{2}})$, are given by:

$$\hat{u}_{r1}(r; r_c) = a_0^- r^{m-1} + \frac{(1 - a_0^-)}{r^{m+1}}, \tag{3.65}$$

$$\hat{u}_{r2}(r; r_c) = \frac{b_0^+}{r^{m+1}}, \tag{3.66}$$

where a_0^- and b_0^+ have been defined in terms of $\hat{u}_r(r_c; r_c)$ above. The eigenfunction within the elastic boundary layer, again to $O(E^{\frac{1}{2}})$, may be written down in the following piecewise form:

$$u_r^-(\eta) = C_2 \text{Pf}.\eta \ln \frac{\eta - 1}{\eta + 1} + E^{\frac{1}{2}} \eta \Big[C_3^- + \frac{3}{\sqrt{2} r_c} C_2 \text{Pf}. \left(\eta \ln \frac{\eta - 1}{\eta + 1} - \frac{2}{\eta^2 - 1} \right) \Big] \quad \eta < -1, \tag{3.67}$$

$$u_r(\eta) = \eta \Big[C_1 + C_2 \text{Pf}.\eta \ln \frac{1 - \eta}{1 + \eta} \Big] + E^{\frac{1}{2}} \eta \Big[C_3 + \frac{3}{\sqrt{2} r_c} C_2 \text{Pf}. \left(\eta \ln \frac{1 - \eta}{1 + \eta} - \frac{2}{\eta^2 - 1} \right) \Big] \quad -1 < \eta < 1, \tag{3.68}$$

$$u_r^+(\eta) = C_2 \text{Pf}.\eta \ln \frac{\eta - 1}{\eta + 1} + E^{\frac{1}{2}} \eta \Big[C_3^+ + \frac{3}{\sqrt{2} r_c} C_2 \text{Pf}. \left(\eta \ln \frac{\eta - 1}{\eta + 1} - \frac{2}{\eta^2 - 1} \right) \Big] \quad \eta > 1. \tag{3.69}$$

Note that the terms linear in η, at leading order and at $O(E^{\frac{1}{2}})$, have been combined into a single term, $C_1 \eta$, in (3.68). While $C_2 = -\frac{\hat{u}_r(r_c; r_c)}{2}$, and $C_3^{\pm}$ in the above expressions are given by (3.63) and (3.64), respectively, C_1 in (3.68) remains arbitrary. The prefix Pf. in (3.67)-(3.69) denotes a principal-finite-part interpretation which, as will be seen below (and as already seen when analyzing the perturbation vorticity in elastic Couette flow in chapter 2), is required in interpreting the axial vorticity field within the elastic boundary layer. The expressions (3.67)-(3.69), taken together with the expressions for the constants involved, show that the CS-modes for small but finite E involve two parameters. These may be taken as $[\hat{u}_r(r_c; r_c) - r_c^{-(m+1)}]$ and C_1, where $1/r_c^{(m+1)}$ is the normalized radial velocity associated with the Kelvin mode at $r = r_c$. The first parameter, of course, already exists for $E = 0$, and is proportional to the amplitude of the second vortex sheet, $A(r_c)$, used earlier for the description of the CS-modes for $E = 0$ (see (3.16)-(3.19). The second parameter arises only for non-zero E and affects the detailed structure of the (elastic) boundary layer vorticity field.

The finite-E generalization of the regular Kelvin mode may be obtained by taking $r_c = r_{ck}, a_0^- = 0, b_0^- = 1$. This implies $C_2 = -1/(2r_{ck}^{(m+1)}), C_3^- = C_3^+ = -(2m+5)/(\sqrt{2} r_{ck}^{(m+2)})$. The

$O(\sqrt{E})$ elastic boundary layer constants, C_3^+ and C_3^-, play a crucial role in sensing the different modes associated with the Rankine vortex, and their equality ensures an identical slope of the radial velocity field on either side of the elastic boundary layer. In the outer region, one now has $\hat{u}_{r1}(r; r_c) = \hat{u}_{r2}(r; r_c) = 1/r^{(m+1)}$, and within the boundary layer, (3.16)-(3.19) take the form:

$$u_{rk}^-(\eta) = -\frac{1}{2r_{ck}^{(m+1)}}\text{Pf.}\eta\ln\frac{\eta-1}{\eta+1} + \frac{E^{\frac{1}{2}}\eta}{\sqrt{2}r_{ck}^{(m+1)}}\left[(2m+5) + \frac{3}{2}\text{Pf.}\left(\eta\ln\frac{\eta-1}{\eta+1} - \frac{2}{\eta^2-1}\right)\right] \quad \eta < -1, \tag{3.70}$$

$$u_{rk}(\eta) = \eta\Big[C_1 - \frac{1}{2r_{ck}^{(m+1)}}\text{Pf.}\ln\frac{1-\eta}{1+\eta}\Big] + \frac{3E^{\frac{1}{2}}\eta}{2\sqrt{2}r_{ck}^{(m+1)}}\text{Pf.}\left(\eta\ln\frac{1-\eta}{1+\eta} - \frac{2}{\eta^2-1}\right) \quad -1 < \eta < 1, \tag{3.71}$$

$$u_{rk}^+(\eta) = -\frac{1}{2r_{ck}^{(m+1)}}\text{Pf.}\eta\ln\frac{\eta-1}{\eta+1} - \frac{E^{\frac{1}{2}}\eta}{\sqrt{2}r_{ck}^{(m+1)}}\left[(2m+5) + \frac{3}{2}\text{Pf.}\left(\eta\ln\frac{\eta-1}{\eta+1} - \frac{2}{\eta^2-1}\right)\right] \quad \eta > 1, \tag{3.72}$$

The above expressions suggest that the finite-E generalization of the regular Kelvin mode is a one-parameter family of singular eigenfunctions, C_1 being the parameter, with singularities at $r = r_c \pm \sqrt{2E}(\eta = \pm 1)$ for small E.

3.4.3 Perturbation vorticity field

The interpretation of the Kelvin mode for finite E in the previous section also becomes clear on consideration of the axial vorticity field associated with (3.67)-(3.69) (recall that the velocity field in the outer regions is irrotational to $O(E^{\frac{1}{2}})$. For $E = 0$, the axial vorticity field is, of course, a delta function at $r = r_c$. For small but finite E, the vorticity field is still localized within the elastic boundary layer which may therefore be regarded as a vortex sheet on the scale of the outer region. One may therefore discriminate between the 2D CS-modes and Kelvin mode based on the strength of this equivalent vortex sheet, defined as the total vorticity contained within the $O(E^{\frac{1}{2}})$ boundary layer over a single wavelength in the azimuthal direction. We have the following expression for the perturbation axial vorticity eigenfunction in terms of the radial velocity $\tilde{u}_r(r)$:

$$\hat{\omega}_z(r) = -\nabla_r^2\psi = \frac{i}{m}[\nabla_r^2(r\tilde{u}_r)], \tag{3.73}$$

where ψ is the stream function, ∇_r^2 representing the Laplacian in radial co-ordinates both given by relations:

$$\psi = -\frac{i(r\tilde{u}_r)}{m} \quad \text{and} \quad \nabla_r^2 = \frac{\partial^2}{\partial r^2} + \frac{1}{r}\frac{\partial}{\partial r} - \frac{m^2}{r^2} \tag{3.74}$$

One obtains:

$$\hat{\omega}_z(r) = \frac{i}{m}\Big[r\frac{\partial^2 \tilde{u}_r}{\partial r^2} + 3\frac{\partial \tilde{u}_r}{\partial r} - \frac{(m^2-1)\tilde{u}_r}{r}\Big], \tag{3.75}$$

or, in terms of the boundary layer variable (η):

$$\tilde{\omega}_z(\eta) \approx \frac{i}{m}\Big\{r_c\frac{\partial^2 \tilde{u}_r}{\partial \eta^2} + \sqrt{E}\Big\{\sqrt{2}\eta\frac{\partial^2 \tilde{u}_r}{\partial r^2} + 3\sqrt{2}\frac{\partial \tilde{u}_r}{\partial \eta}\Big\}\Big\} \tag{3.76}$$

where $\tilde{\omega}_z(\eta) = (2E)\hat{\omega}_z(r)$. Now, consider the expansion, $\tilde{u}_r = u_r^{(0)} + \sqrt{E}u_r^{(1)} + \cdots$ and $\tilde{\omega}_z = \tilde{\omega}_z^{(0)} + \sqrt{E}\tilde{\omega}_z^{(1)} + \cdots$ On substituting in the above expression for the vorticity eigenfunction, we have following expression for the vorticity field:

$$\begin{aligned}\tilde{\omega}_z^{(0)}(\eta) &= \frac{i}{m}\Big[r_c\frac{\partial^2 \tilde{u}_r^{(0)}}{\partial \eta^2}\Big], &(3.77)\\ &= \frac{i}{m}\Big[-\text{Pf.}\frac{4C_2}{(\eta^2-1)^2} + C_1[\delta(\eta+1) - \delta(\eta-1) + \delta'(\eta+1) + \delta'(\eta-1)]\Big], &(3.78)\end{aligned}$$

at leading order, with Pf. denoting a principal-finite-part interpretation, and:

$$\begin{aligned}\tilde{\omega}_z^{(1)}(\eta) = \frac{i}{m}\Big[\underbrace{\eta\sqrt{2}\frac{\partial^2 u_{r0}}{\partial \eta^2} + 3\sqrt{2}\frac{\partial u_{r0}}{\partial \eta}}_{O(1)\text{velocity contribution}} + r_c\frac{\partial^2 u_{r1}}{\partial \eta^2}\Big],\\ = P\frac{iC_2}{m}\Big[\sqrt{2}\Big(\frac{2\eta(3\eta^2-5)}{(\eta^2-1)^2} + 3\ln\Big|\frac{\eta-1}{\eta+1}\Big|\Big) + 2r_c\Big(\ln\Big|\frac{\eta-1}{\eta+1}\Big| + \frac{2\eta(\eta^4-4\eta^2-1)}{(\eta^2-1)^3}\Big)\Big]\\ + \frac{ir_c}{m}\Big[C_1^-\Big\{\delta'(\eta+1) - \delta(\eta+1)\Big\} + C_1^+\Big\{\delta'(\eta-1) + \delta'(\eta+1)\Big],\end{aligned} \tag{3.79}$$

at $O(E^{\frac{1}{2}})$. Here, 'P' denotes a Cauchy-principal-value interpretation. This ensures that the contributions that are odd in η, corresponding to jet-like structures either localized at the travelling wave singularities (proportional to $\delta'(\eta \pm 1)$), or non-local but within the elastic boundary layer, are negligibly small for $E \ll 1$.

The total boundary layer vorticity over half a wavelength in the azimuthal direction may be given by integrating the vorticity eigenfunction with respect to the radial coordinate. Thus, we have for the boundary layer vorticity:

$$\int_{r_c-O(1)}^{r_c+O(1)} \hat{\omega}_{z(r)} r dr, \quad = \quad 2\pi\int_{r_c-O(1)}^{r_c+O(1)} \hat{\omega}_{z(r)} r dr, \tag{3.80}$$

and on transforming the variable, we have

$$\omega_z(\eta) = 2\pi \int_{-\infty}^{+\infty} \hat{\omega}_z(\eta)[r_c + \eta\sqrt{2E}]\sqrt{2E}d\eta \quad \text{where} \quad \eta = \frac{r - r_c}{\sqrt{2E}} \tag{3.81}$$

The integrated boundary-layer vorticity, for small E, may be written as:

$$\begin{aligned} \omega_z(\eta) &= E^{\frac{1}{2}}\Big\{2\sqrt{2}\pi r_c \int_{-\infty}^{+\infty} \tilde{\omega}_{z0} d\eta\Big\} + E\Big\{4\pi \int_{-\infty}^{+\infty} \tilde{\omega}_{z0}\eta d\eta + 2\sqrt{2}\pi r_c \int_{-\infty}^{+\infty} \tilde{\omega}_{z1} d\eta\Big\}, && (3.82) \\ &= -\frac{8i\pi r_c^2 C_2}{m(2E)^{\frac{1}{2}}} \quad \text{Pf.} \int_{-\infty}^{+\infty} \frac{d\eta}{(\eta^2-1)^2} + \frac{ir_c}{m}(C_3^+ - C_3^-) + O(E^{\frac{1}{2}}) && (3.83) \\ &= \frac{ir_c}{m}(C_3^+ - C_3^-) + O(E^{\frac{1}{2}}) && (3.84) \end{aligned}$$

The principal-finite-part integral in (3.83) is identically zero, and thus the boundary layer vorticity is proportional to $C_3^+ - C_3^-$. This difference between the two boundary layer constants denotes the strength of the elastic boundary layer, when interpreted as an equivalent vortex sheet on the outer length scale scale. This vortex-sheet contribution evidently is present only for the CS-modes, and vanishes for the Kelvin mode in which case $C_3^+ = C_3^-$. The equivalent circumstance, that given by $B_1^+ = B_1^-$, never occurs for plane Couette flow owing to the purely continuous nature of the original inviscid spectrum.

Having established in detail a connection between the solutions of the elastic Rayleigh equation for small but finite E, and the original inviscid spectrum of the Rankine vortex (including the Kelvin mode), we proceed towards an alternate intepretation of the CS-eigenfunctions for non-zero E. As will be seen, this interpretation is more general in that it is not reliant on E being small. The presence of two parameters, $[\hat{u}_r(r; r_c) - 1/r_c^{m+1}]$ and C_3 in (3.65)-(3.69), implies the existence of a pair of continuous spectra for finite E, in contrast to the single one for $E = 0$. It is convenient to regard each of these as corresponding to a particular choice of C_3 in (3.68), and therefore, as being parameterized by $[\hat{u}_r(r; r_c) - 1/r_c^{m+1}]$ alone. The natural choices are $C_3 = E^{\frac{1}{2}}C_3^+$ and $C_3 = E^{\frac{1}{2}}C_3^-$ which ensure the smooth connection of the regular solution across $\eta = 1$ and -1, respectively. For either choice, the absence of a kink ensures the absence of delta-function-like contributions to the tangential velocity and vorticity fields at the relevant travelling wave singularity. Of course, the finite-E eigenfunction is still singular owing to the logarithmic terms in (3.67)-(3.69). From here onwards, the singularities at $\eta = 1$ and -1 will be associated with the fast (or forward) and slow (or backward) shear wave, respectively, for obvious reasons. The choice $C_3 = C_3^+$ implies that one only has a kink at the slow shear wave. Since it is this kink that allows for singular eigenfunctions even as r_c spans a continuous interval, the interval of existence for this slow-shear-wave-spectrum (SSWS) may be obtained by the requirement that the kink (the location of the slow shear wave singularity) lie in the physical domain. The slow shear wave propagates with an angular frequency of $\omega = m[\Omega(r) + \Omega'(r)(2E)^{\frac{1}{2}}] = m[1/r^2 - 2(2E)^{\frac{1}{2}}/r^3]$, which must then lie in the base-state range of angular frequencies (0, m). The shear wave frequency evidently approaches zero for $r \rightarrow \infty$, while it equals m for $r = r_{cs}$ with $[1/r_{rs}^2 - 2(2E)^{\frac{1}{2}}/r_{rs}^3] = 1$. For small E this gives $r_{cs} = 1 - (2E)^{\frac{1}{2}}$, corresponding to an angular frequency of $(1+2(2E)^{\frac{1}{2}})$. So, the SSWS frequency interval is $[0, m(1+2(2E)^{\frac{1}{2}})]$. Analogous arguments for the fast shear wave yield the frequency interval for the fast-shear-wave-spectrum (FSWS) as $[0, m(1-2(2E)^{\frac{1}{2}})]$ for small E. The SSWS and FSWS eigenfunctions differ in structure only within the $O(E^{\frac{1}{2}})$ boundary layer, where they are given by:

$$u_r^-(\eta) = C_2\text{Pf.}\eta\ln\frac{\eta-1}{\eta+1} + E^{\frac{1}{2}}\eta\Big[C_3^- + \frac{3}{\sqrt{2}r_c}C_2\text{Pf.}\left(\eta\ln\left|\frac{\eta-1}{\eta+1}\right| - \frac{2}{\eta^2-1}\right)\Big] \quad \eta < -1, \tag{3.85}$$

$$u_r^+(\eta) = C_2\text{Pf.}\eta\ln\left|\frac{\eta-1}{\eta+1}\right| + E^{\frac{1}{2}}\eta\Big[C_3^+ + \frac{3}{\sqrt{2}r_c}C_2\text{Pf.}\left(\eta\ln\frac{\eta-1}{\eta+1} - \frac{2}{\eta^2-1}\right)\Big] \quad \eta > -1, \tag{3.86}$$

and

$$u_r^-(\eta) = C_2\text{Pf.}\eta\ln\left|\frac{\eta-1}{\eta+1}\right| + E^{\frac{1}{2}}\eta\Big[C_3^- + \frac{3}{\sqrt{2}r_c}C_2\text{Pf.}\left(\eta\ln\left|\frac{\eta-1}{\eta+1}\right| - \frac{2}{\eta^2-1}\right)\Big] \quad \eta < 1, \tag{3.87}$$

$$u_r^+(\eta) = C_2\text{Pf.}\eta\ln\frac{\eta-1}{\eta+1} + E^{\frac{1}{2}}\eta\Big[C_3^+ + \frac{3}{\sqrt{2}r_c}C_2\text{Pf.}\left(\eta\ln\frac{\eta-1}{\eta+1} - \frac{2}{\eta^2-1}\right)\Big] \quad \eta > 1, \tag{3.88}$$

respectively, to $O(E^{\frac{1}{2}})$. The SSWS interval above extends outside the base-state interval of angular frequencies, clearly implying that the modified semi-circle theorem stated earlier does not apply to the CS-modes. The purely inviscid case, in having the CS-interval equal to the semi-circle radius, is, in fact, a little misleading in this regard! It is worth noting that the expressions (3.87)-(3.88) are valid only when the elastic boundary layer is an $O(1)$ distance away from the core.

The point that needs emphasis, with regard to the alternate interpretation above, is its validity for arbitrary E. Although closed form expressions for the eigenfunctions, belonging to the two continuous spectra, can no longer be obtained when E is not small, the pair of travelling wave singularities still exist and satisfy $\omega = m[\Omega(r) \pm 2\Omega'(r)(2E)^{\frac{1}{2}}]$. The elastic boundary layer solution given in (3.41) must now be interpreted as a Frobenius expansion in the vicinity of the relevant singular point. The FSWS spectrum corresponds to the interval $[0, m(1-2(2E)^{\frac{1}{2}})]$ for $E < 1/8$, and to $[m(1-2(2E)^{\frac{1}{2}}), 0]$ for $E > 1/8$. The SSWS spectrum continues to be given by $[0, m(1+2(2E)^{\frac{1}{2}})]$ for finite E, although there arises a degeneracy for $E > 1/18$ due to shear waves at a pair of radial locations propagating with the same frequency.

The CS-modes arising from the multiple continuous spectra above, together with a finite number of discrete modes, must form a complete basis for the independent fields required to completely characterize an initial state in the limit $Re, De \to \infty$. For the Rankine vortex, as governed by the elastic Rayleigh equation, these may be taken as the radial velocity field and the two components of the polymeric force field $(\nabla.\mathbf{a})$; since the radial component of the normal stress (a_{rr}) does not enter in the elastic Rayleigh limit, one may equivalently consider the radial velocity field and the stress components $a_{r\theta}$ and $a_{\theta\theta}$. One therefore needs (at least) three continuous spectra in order to represent an arbitrary initial condition. The analysis detailed above, in choosing a continuous solution across $r = r_c(\eta = 0)$, does not account for the third spectrum needed. As discussed briefly earlier, this is the Doppler spectrum corresponding to $\omega = \Omega(r_c)$. Although $r = r_c$ is an ordinary point for the elastic Couette flow, in a manner similar to inviscid plane Couette flow (Case (1960)), one nevertheless requires CS-modes with a singularity at $r = r_c$ to generate a complete basis. In the limit under consideration, that of finite E, with $De \to \infty$, the Doppler-spectrum eigenfunctions may be generated by different choices of one of the two regular solutions,(the one corresponding to a Frobenius exponent of 0) on either side of $r = r_c$.

3.4.4 Uniformly valid analysis

In the last section, we have solved the problem in the framework of matched asymptotic expansions approach in the case where the elastic boundary layer lies an $O(1)$ distance away from the edge of the core. In the present section, we briefly discuss the uniformly valid solution that becomes necessary when the critical radius (r_c) is within an $O(E^{\frac{1}{2}})$ distance from the core. This approach becomes necessary when obtaining the eigenfunctions close to the edge of the continuous spectrum (defined as eigenfunctions with angular frequencies that are within $O(E^{\frac{1}{2}})$ of the core angular frequency). In this case, one only has an outer inviscid region and the core boundary condition has to directly be imposed on the elastic boundary layer solution. Thus, we start with the outer inviscid solution and the inner boundary layer and implement both the matching and core conditions. The expressions (3.51) and (3.65) give the required asymptotic forms of the inner and outer solutions, respectively. Considering $a_0 = 1$ and $b_0' = b_0/a_0$, on matching the two solutions in the respective limits, we have:

$$\begin{aligned} C_1^- &= (m-1)r_c^{(m-2)}\sqrt{2E} - b'(m+1)r^{-(m+2)}\sqrt{2E} \\ C_2^- &= -\Big(\frac{r_c^{(m-1)} + b' r_c^{-(m+1)}}{2}\Big) \end{aligned} \tag{3.89}$$

With inner and outer leading order solutions at hand, we adopt the method of constructing the composite solution from Dyke (1975). The common part of the inner and outer solutions can be found from matching, and is give by, $-2C_2^- + \eta C_1^-$. Hence, the final expression for the uniform solution reduces to:

$$u_r(r) = r^{(m-1)} + b_0' r^{-(m+1)} + \Big(\frac{r-r_c}{\sqrt{2E}}\Big)\Big[C_1^- + C_2^- \ln\left|\frac{r-r_c+\sqrt{2E}}{r-r_c-\sqrt{2E}}\right|\Big] + 2C_2^- - \Big(\frac{r-r_c}{\sqrt{2E}}\Big)C_1^- \tag{3.90}$$

With C_1^- and C_2^- given by (3.89). One can easily see that in the limit $(r-r_c) \sim O(E^{\frac{1}{2}})$, the above solution reduces to the outer inviscid solution and for the case where $(r-r_c) \rightarrow O(1)$, it reduces to the inner boundary layer solution. The above solution satisfies the core boundary condition,$(u_r(1) = 1)$, provided.

$$\Rightarrow b_0' = \Bigg[\frac{r_c^{(m-1)}\Big\{1 + \frac{(1-r_c)}{2\sqrt{2E}} \ln\left|\frac{1-r_c+\sqrt{2E}}{1-r_c-\sqrt{2E}}\right|\Big\}}{1 - r_c^{-(m+1)}\Big\{1 + \frac{(1-r_c)}{2\sqrt{2E}} \ln\left|\frac{1-r_c+\sqrt{2E}}{1-r_c-\sqrt{2E}}\right|\Big\}}\Bigg] \tag{3.91}$$

For $(r-r_c) \rightarrow O(1)$ (the inviscid regime), b_0' reduces to 0, satisfying wall condition. Hence the uniformly valid solution associated with left-travelling wave singularity have the form given by (3.90) with b_0' given by (3.91).

3.5 Conclusion

In this chapter, we examined in some detail the spectral characteristics of elastic Rayleigh equation which governs the evolution of small-amplitude two-dimensional perturbations, to a base-state swirling flow, in the limit Re and $De \rightarrow \infty$. The effects of elasticity were examined analytically via a matched asymptotic expansions approach in the limit of small but finite E. It was thereby shown that, in addition to the elastically modified version of the Doppler spectrum associated with the original inviscid Rayleigh equation, that spans the base-state range of velocities, the elastic Rayleigh equation exhibits an additional pair of continuous spectra that may be associated with singular neutrally stable *slow* and $fast$ elastic shear waves propagating with speeds proportional to $\pm\sqrt{2E}$ relative to the local flow. The singular eigenfunctions associated with these travelling-wave spectra exhibit an elastic boundary layer with a thickness of $O(E^{\frac{1}{2}})$ about the original critical-level, where elasticity and inertia are comparable. In contrast to the original inviscid eigenfunctions that exhibit only a kink in the radial velocity field, the radial velocity field exhibits a logarithmic divergence at a pair of locations within this elastic boundary layer. The axial vorticity field is more singular, and requires a principle-finite-part-interpretation. The analysis for small E also showed that the original inviscid Kelvin mode was replaced by a one-parameter family of singular elastic modes.

Chapter 4

Finite De analysis

4.1 Introduction

Having studied how the presence of elasticity modifies the inviscid continuous spectrum, in previous chapters, for both the plane Couette (Chapter 2) and the Rankine vortex (Chapter 3) profiles, in the limit $De \to \infty$ with the effects of microstructural relaxation being neglected, we now intend to look at the additional effects caused by the inclusion of weak relaxation effects. For this purpose we study plane Couette flow alone, but based on the extended equation (see 2.10 in Chapter 2), in the limit of De being large but finite. This equation may again be written as:

$$\Big[y_*^2 D^2 - 2Dy_* + 2 - k^2 y_*^2\Big]\Big[D^2 + 2ikDeD - k^2(1+2De^2)\Big]\hat{u}_y(y) = \\ -ikDe\Big(\frac{\beta}{1-\beta}\Big)y_*^3(D^2-k^2)^2\hat{u}_y - k^2(Re.De)\Big(\frac{\beta}{1-\beta}\Big)y_*^3(y-c)(D^2-k^2)\hat{u}_y(y), \quad (2.10)$$

where $y_* = \frac{\Sigma_2}{ik} = y - c - \frac{i}{kDe}$ and $D = d/dy$. Here, $\beta = 0$ corresponds to a UCM fluid while $\beta = 1$ corresponds to a Newtonian fluid. Recall that (2.10) is the viscoelastic analog of the Orr-Sommerfeld equation for plane parallel shearing flows of a Newtonian fluid, and for a fixed β, the evolution of perturbations, as governed by (2.10), depends therefore on both Re and De. Equation (2.10), in the above form, has been obtained earlier; see, for instance, Kumar & Shankar (2005). As discussed earlier in chapter 2, (2.10), for finite De, supports a pair of continuous spectra (Wilson *et al.* (1999); Kupferman (2005)) in addition to the discrete modes. For $\beta = 0$ (the UCM limit), and $Re \to 0$, the spectrum of (2.10) in plane Couette flow was first characterized by Gorodtsov and Leonov (Gorodtsov & Leonov (1967)). It consists of two discrete eigenvalues, and a continuous spectrum given by $c = y + \frac{i}{k\,De}$ with $y \,\epsilon\, [0,1]$. For $\beta \neq 0$, corresponding to an Oldroyd-B fluid, there arises an additional viscous continuous spectrum given by $c = y + \frac{i}{k\beta\,De}$, $y \,\epsilon\, [0,1]$, together with a finite number of discrete eigenvalues; the number of discrete viscous eigenvalues tends to infinity in the UCM limit $\beta \to 0$ (Wilson *et al.* (1999)).

From what is known about the eigenfunctions of the Rayleigh and Orr-Sommerfeld equations (see section 5 in Roy & Subramanian (2014*b*)), one expects a non-trivial relationship between the spectrum of the elastic Rayleigh equation (equation (.) in chapter[2]), and that for large but finite De (equation (2.10) above). The phrase 'non-trivial' is used here in the sense that there may not be a one-to-one correspondence between the $De = \infty$ eigenfunctions and those for $De \gg 1$. For instance, each inviscid elastic eigenfunction of the elastic Rayleigh equation may arise as an infinite superposition of eigenfunctions of (2.10) even as $De \to \infty$. To examine this relation, we now consider (2.10) which governs the evolution of elastic perturbations in Couette flow.

For purposes of simplicity, we restrict ourselves to the case $\beta = 0$, neglecting the direct effects of solvent viscosity, and thereby avoid additional complications associated with the viscous continuous spectrum. In the foregoing chapters, we have characterized the three continuous spectra associated with the elastic Rayleigh equation for a pair of canonical base-state velocity profiles - one associated with the critical level, and the two associated with the pair of travelling wave singularities. The objective now is to see how each of these spectra is affected by weak relaxation effects. It is found below that the critical-level singularity and the associated continuous spectrum survives at large but finite De, since the elastic part of (2.10) continues to support a continuous spectrum (the GL spectrum) for any finite De with $\beta = 0$. When De is large, the second order derivatives in this elastic part begin to dominate the fourth-order ones except in an asymptotically thin relaxation boundary layer around the critical level. It is thus found that outside an $O(De^{-1})$ inner boundary layer around the critical point, within which the fourth-order terms are still important, the second-order terms dominate with (apparent) Frobenius exponents of 1 and 2. These exponents were identified in chapter 3, and are determined only by the elastic part of the Rayleigh operator. In contrast, (2.10) is not singular at the travelling wave locations, and therefore, the travelling-wave spectra identified in the elastic Rayleigh limit cannot persist at finite De however large. We explore the possibility below of the singular travelling-wave eigenfunctions being regularized locally, within an inner relaxation boundary layer, with the original singularity being resolved into a small-scale oscillation in the relaxation region. The analysis in section 4.1.2 shows that this does not happen, and that the effects of relaxation must therefore be global in nature (much like a weak viscosity leads to the existence of the viscous solutions of the Orr-Sommerfeld equation [Drazin & Reid (1981)]).

4.1.1 Boundary layer analysis at the critical level

With a little analysis it may be shown that there exists an inner relaxation boundary layer of thickness $O(1/De)$, around the critical-level (with $De^{-1} \ll E^{\frac{1}{2}}$, or equivalently, $Re \ll De^3$) where relaxation terms become important. Within this $O(De^{-1})$ layer, the elastic terms in the original elastic Rayleigh operator balance the relaxation terms at leading order; next, within a larger boundary layer with thickness of $O(E^{\frac{1}{2}})$, there is the balance between elastic and inertial terms already seen in earlier chapters, and finally, the inviscid inertial solution is dominant in the domain outside the boundary layer. This makes up the layered asymptotic structure characterizing an eigenfunction with a singularity at the critical-level in the limit $De, Re \gg 1$ and with $Re \ll De^3$.

The factor responsible for the GL spectrum in (2.10) is $y^* = y - c - \frac{i}{kDe}$. With $c = c_r + ic_i$, and $c_i = \hat{c}_i/De$, $\hat{c}_i \sim O(1)$, we have $y - c - \frac{i}{kDe} = y - c_r - i[\hat{c}_i + (1/k)]/De$. With $\hat{c}_i = -1/k$, and $\hat{Y} = De(y - c_r)$ being the new boundary layer variable, we have the following fourth-order equation valid around the critical-level at leading order:

$$\left[\hat{Y}^2 D^2 - 2\hat{Y} D + 2\right]\left[D^2 + 2ikD - 2k^2\right] u_y(\hat{y}) = 0 \qquad (4.1)$$

where $D \equiv \frac{d}{d\hat{Y}}$. The above equation represents the local form of the original equation considered by Gorodtsov and Leonov (Gorodtsov & Leonov (1967)) and Wilson (Wilson *et al.* (1999)) for inertialess plane Couette flow. The solution to the above equation takes the form:

$$u_y(\hat{y}) = B_3\left\{\exp(-k\hat{Y}(1+i))\right\} + B_4\left\{\exp(k\hat{Y}(1-i))\right\} - B_5\left\{\frac{i + k\hat{Y}}{2k^3}\right\} + B_6\left\{\frac{1 - 2ik\hat{Y} - k^2\hat{Y}^2}{2k^4}\right\} \qquad (4.2)$$

Here, the four independent solutions are the local representations, for $y \to y_c$, of the solutions derived by Graham in the appendix of Graham (1998) (also see Miller (2005)). To eliminate exponential growth for large $|\hat{Y}|$, one sets $B_3 = 0$ for $\hat{Y} > 0$ and $B_4 = 0$ for $Y < 0$. The two algebraically growing solutions on either side of $\hat{Y} = 0$, for $|\hat{Y}| \to \infty$, match up to the solutions of the elastic Rayleigh equation for $\xi \to 0$ (ξ being the variable in the $O(E^{\frac{1}{2}})$ elastic boundary layer analyzed in Chapter 2); the third exponentially decaying solution does not enter the matching procedure. It may be shown that the constants multiplying these algebraic solutions on either side of the critical level, $B_5^{\pm}$ and $B_6^{\pm}$, may thereby be determined. Owing to the differing constants on either side of the critical level, the large-but-finite De eigenfunction remains singular in the vicinity of the critical level, and the nature of the singularity, within the inner $O(De^{-1})$ relaxation layer, is identical to that identified earlier for the viscoelastic continuous spectrum in inertialess flows.

4.1.2 Boundary layer analysis at travelling waves locations

Unlike the finite-De critical level spectrum analyzed above, the travelling-wave spectra arise due to a balance of inertial and elastic terms. With the inclusion of relaxation terms, $y = c \pm \sqrt{2E}$ no longer correspond to singular locations, and the travelling-wave spectra must therefore disappear for any finite De. Instead, there exists a boundary layer with thickness of $O(\frac{E^{1/4}}{De^{1/2}})$ around each of these singular locations in which the inertial, elastic and relaxation terms balance at leading order,(the requirement that these boundary layers be small compared to the $O(E^{\frac{1}{2}})$ inviscid elastic boundary layer encountered earlier leads to the same condition, $Re \ll De^3$, as for the relaxation layer around the critical-level singularity). Considering the boundary layer around the slow-shear-wave singularity at $y = c - \sqrt{2E}$, we introduce a boundary layer variable ζ defined as:

$$\zeta = \left[y - (c - \sqrt{2E})\right] \frac{De^{1/2}}{E^{1/4}} \tag{4.3}$$

On substituting, (2.10) can then be written in the following reduced form at leading order $(O(E^{5/4}De^{1/2}))$:

$$\left[D^3 + ik\sqrt{2}\zeta D^2 + i\sqrt{2}kD\right] u_y(\zeta) = 0, \tag{4.4}$$

where $D \equiv \frac{d}{d\zeta}$, and the solution to the above equation is given by:

$$u_y(\zeta) = B_{4L} + B_{5L}\Big\{\sqrt{\pi/k}(-2)^{(-3/4)} Erfi\Big[-(-1/2)^{(1/4)}\sqrt{k}\zeta\Big]\Big\} + B_{6L}\Big\{(\frac{\zeta^2}{2})2F_2\Big[(1,1),(\frac{3}{2},2),-\frac{ik\zeta^2}{\sqrt{2}}\Big]\Big\} \tag{4.5}$$

Here, $2F_2[.]$ is the generalized Hypergeometric function, and $Erfi[.]$ denotes the imaginary Error function (see Frank W. J. Olver (2010)).

In an analogous manner, for the fast-shear-wave at $y = c + \sqrt{2E}$, we introduce the boundary

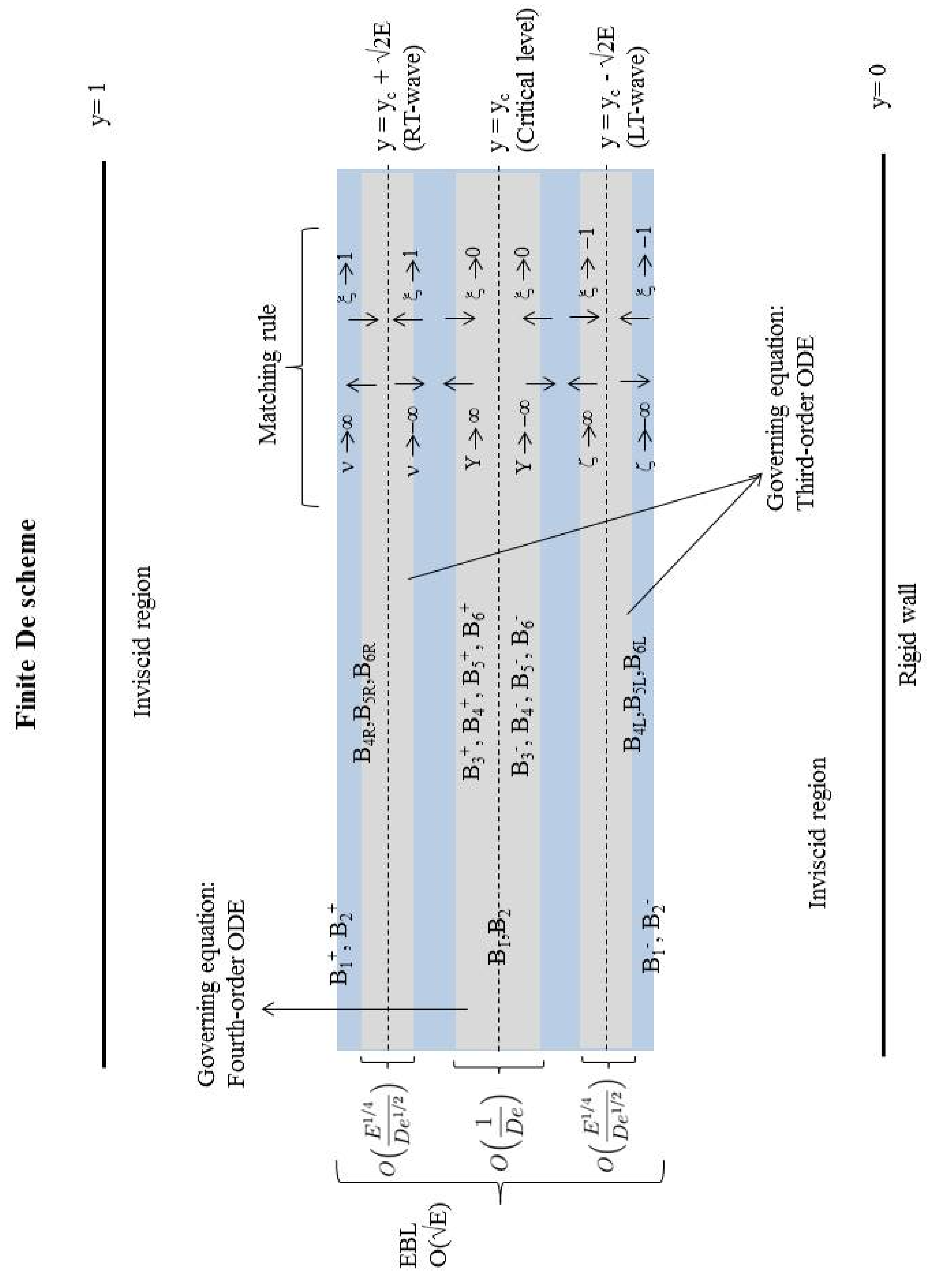
Finite De scheme
y= 1
Inviscid region
Governing equation: Fourth-order ODE
Matching rule
ν → ∞
ν → −∞
Y → ∞
Y → −∞
ζ → ∞
ζ → −∞
ξ → 1
ξ → 0
ξ → −1
B1+ ; B2+
B4R;B5R;B6R
B1;B2
B3+ ; B4+ ; B5+ ; B6+
B3- ; B4- ; B5- ; B6-
B1- ; B2-
B4L;B5L;B6L
y = yc + √2E (RT-wave)
y = yc (Critical level)
y = yc - √2E (LT-wave)
Governing equation: Third-order ODE
Inviscid region
Rigid wall
y= 0
O(E^{1/4}/De^{1/2})
O(1/De)
O(E^{1/4}/De^{1/2})
EBL O(√E)

Figure 4.1: Finite De scheme

layer variable ν, defined as:

$$\nu = \Big[y - (c + \sqrt{2E})\Big] \frac{De^{1/2}}{E^{1/4}} \tag{4.6}$$

On substituting, (2.10) can then be written in the following reduced form at leading order:

$$\Big[D^3 - ik\sqrt{2}\nu D^2 - i\sqrt{2}kD\Big] u_y(\nu) = 0 \tag{4.7}$$

where $D \equiv \frac{d}{d\nu}$. The above equation has a solution of the form:

$$u_y(\nu) = B_{4R} + B_{5R}\Big\{\sqrt{\pi/k}(-2)^{(-3/4)} Erfi\Big[(-1/2)^{(1/4)}\sqrt{k}\nu\Big]\Big\} + B_{6R}\Big\{(\frac{\nu^2}{2})2F_2\Big[(1,1),(\frac{3}{2},2),\frac{ik\nu^2}{\sqrt{2}}\Big]\Big\} \tag{4.8}$$

4.1.3 Matching at the travelling-wave singularities

For purposes of matching, we now write down the expressions for the constants, $B_1^{\pm}$ and B_2, from chapter 2, that appeared in the boundary layer solution of the elastic Rayleigh equation:

$$\begin{aligned} B_1^- &= A^{(-)}(k\sqrt{2E})\cosh[ky_c] \\ B_1^+ &= -A^{(+)}(k\sqrt{2E})\cosh[k(1-y_c)] \\ B_2 &= -\frac{A^{(+)}\sinh[k(1-y_c)]}{2} \quad \text{or} \quad -\frac{A^{(-)}\sinh[ky_c]}{2} \end{aligned} \tag{4.9}$$

The far-field forms of the relaxation layer solutions, in the vicinity of the slow-shear-wave singularity, given by (4.5), are:

$$\begin{aligned} u_y(\zeta)|_{\zeta\to\infty} = B_{4L} + B_{5L}\Big\{\sqrt{\pi/k}(-2)^{(-3/4)}\Big[\frac{(1-i)(-i)^{1/2}}{\sqrt{2}} + O(\frac{1}{\zeta^2})\Big] + \exp(\frac{ik\zeta^2}{\sqrt{2}})\Big[\frac{i(-2)^{1/4}}{\zeta\sqrt{\pi k}} + O(\frac{1}{\zeta^3})\Big]\Big\} \\ +B_{6L}\Big\{\Big[-\frac{i(1+3\log 2+2\log(ik)-4\log(1/\zeta))}{4\sqrt{2}k} + O(\frac{1}{\zeta^2})\Big] + \exp-\frac{ik\zeta^2}{2}\Big[\sqrt{-\frac{-i\pi}{\sqrt{2}k^3}}\frac{1}{\zeta} + O(\frac{1}{\zeta^3})\Big]\Big\} \end{aligned} \tag{4.10}$$

$$\begin{aligned} u_y(\zeta)|_{\zeta\to-\infty} = B_{4L} + B_{5L}\Big\{\sqrt{\pi/k}(-2)^{(-3/4)}\Big[\frac{(i-1)(-i)^{1/2}}{\sqrt{2}} + O(\frac{1}{\zeta^2})\Big] + \exp(\frac{ik\zeta^2}{\sqrt{2}})\Big[\frac{i(-2)^{1/4}}{\zeta\sqrt{\pi k}} + O(\frac{1}{\zeta^3})\Big]\Big\} \\ +B_{6L}\Big\{\Big[-\frac{i(1+3\log 2+2\log(ik)-4\log(1/\zeta))}{4\sqrt{2}k} + O(\frac{1}{\zeta^2})\Big] + \exp-\frac{ik\zeta^2}{\sqrt{2}}\Big[\sqrt{\frac{-i\pi}{\sqrt{2}k^3}}\frac{1}{\zeta} + O(\frac{1}{\zeta^3})\Big]\Big\} \end{aligned} \tag{4.11}$$

The far-field forms of the relaxation layer solutions, in the vicinity of the slow-shear-wave singularity, given by (4.8), are:

$$u_y(\nu)|_{\nu\to\infty} = B_{4R} + B_{5R}\Big\{-\sqrt{\pi/k}(-2)^{(-3/4)}\Big[\frac{(i-1)(-i)^{1/2}}{\sqrt{2}} + O(\frac{1}{\nu^2})\Big] + \exp(\frac{ik\nu^2}{\sqrt{2}})\Big[\frac{(1-i)}{\nu\sqrt{(\sqrt{2}\pi k)}}\Big]\Big\}$$
$$+B_{6R}\Big\{\Big[\frac{i(1+3\log 2+2\log(-ik)-4\log(1/\nu))}{4\sqrt{2}k} + O(\frac{1}{\nu^2})\Big] + \exp\frac{ik\nu^2}{\sqrt{2}}\Big[-\sqrt{\frac{i\pi}{\sqrt{2}k^3}}\frac{1}{\nu} + O(\frac{1}{\nu^3})\Big]\Big\} \tag{4.12}$$

$$u_y(\nu)|_{\nu\to-\infty} = B_{4R} + B_{5R}\Big\{-\sqrt{\pi/k}(-2)^{(-3/4)}\Big[\frac{(i-1)(-i)^{1/2}}{\sqrt{2}} + O(\frac{1}{\nu^2})+\Big] + \exp(\frac{ik\nu^2}{\sqrt{2}})\Big[\frac{(1-i)}{\nu\sqrt{(\sqrt{2}\pi k)}}\Big]\Big\}$$
$$+B_{6R}\Big\{\Big[\frac{i(1+3\log 2+2\log(-ik)-4\log(1/\nu))}{4\sqrt{2}k} + O(\frac{1}{\nu^2})+\Big] + \exp\frac{ik\nu^2}{\sqrt{2}}\Big[\sqrt{\frac{i\pi}{\sqrt{2}k^3}}\frac{1}{\nu} + O(\frac{1}{\nu^3})+\Big]\Big\} \tag{4.13}$$

Before going into the details of finite-De matching associated with the travelling waves, one has to note that the equation governing the $O(\frac{E^{1/4}}{De^{1/2}})$ boundary layer at each of the travelling waves is of third-order and hence involve three finite-De constants, unlike the elastic Rayleigh case where we have two constants. The finite De matching is a two step procedure, where we first match the elastic Rayleigh solutions to the outer inviscid solutions, and then the inner finite-De solutions to the relevant elastic solutions. Here we have the following set of matching requirements (see Fig(4.1)), for matching finite De solutions to elastic solutions:

$$u_y(\nu)|_{\nu\to\infty} \quad \Leftrightarrow \quad \tilde{u}_{y+}(\xi)|_{\xi\to 1} \quad \text{(RT-wave (outer layer))} \tag{4.14}$$

$$u_y(\nu)|_{\nu\to-\infty} \quad \Leftrightarrow \quad \tilde{u}_{y}(\xi)|_{\xi\to 1} \quad \text{(RT-wave (inner layer))} \tag{4.15}$$

$$u_y(\zeta)|_{\zeta\to\infty} \quad \Leftrightarrow \quad \tilde{u}_{y}(\xi)|_{\xi\to -1} \quad \text{(LT-wave (inner layer))} \tag{4.16}$$

$$u_y(\zeta)|_{\zeta\to-\infty} \quad \Leftrightarrow \quad \tilde{u}_{y-}(\xi)|_{\xi\to -1} \quad \text{(LT-wave (outer layer))} \tag{4.17}$$

Matching the slow shear wave solution with the elastic Rayleigh one on the '+′ side gives:

$$B_{6R} = -i\sqrt{2}kB_2 \tag{4.18}$$

$$B_{4R} + B_{5R}\Big\{\frac{-\sqrt{\pi/k}(-2)^{(-3/4)}(i-1)(-i)^{1/2}}{\sqrt{2}}\Big\} + B_{6R}\Big\{\frac{i(1+3\log 2+2\log(-ik))}{4\sqrt{2}k}\Big\}$$
$$= B_1^+ + B_2[(i\pi) - \log 2 + \log(\frac{E^{-1/4}}{De^{1/2}})] \tag{4.19}$$

Matching with the elastic Rayleigh solutions in the central part of the boundary layer gives:

$$B_{6R} = -i\sqrt{2}kB_2 \tag{4.20}$$

$$\begin{aligned}&B_{4R} + B_{5R}\Big\{\frac{\sqrt{\pi/k}(-2)^{(-3/4)}(i-1)(-i)^{1/2}}{\sqrt{2}}\Big\} + B_{6R}\Big\{\frac{i(1+3\log 2+2\log(-ik))}{4\sqrt{2}k}\Big\}\\ &= B_1 + B_2[(i\pi) - \log 2 + \log(\frac{E^{-1/4}}{De^{1/2}})]\end{aligned} \tag{4.21}$$

The above equations give the relation:

$$\begin{aligned}B_1 &= A^+k\sqrt{2E}\cosh[k(1-y_c)] + A^+\sinh[k(1-y_c)]\Big\{i\pi + \log(\frac{E^{-1/4}}{De^{1/2}})\\ &- \log 2 - \frac{(1+3\log 2+2\log(-ik))}{4} + 2B_{4R}\end{aligned} \tag{4.22}$$

Matching the fast shear wave solution with the elastic Rayleigh solution in the central part of the boundary layer gives:

$$B_{6L} = i\sqrt{2}kB_2 \tag{4.23}$$

$$\begin{aligned}&B_{4L} + B_{5L}\Big\{\frac{-\sqrt{\pi/k}(-2)^{(-3/4)}(i-1)(-i)^{1/2}}{\sqrt{2}}\Big\} + B_{6L}\Big\{-\frac{i(1+3\log 2+2\log(ik))}{4\sqrt{2}k}\Big\}\\ &= -B_1 - B_2[\log 2 - \log(\frac{E^{-1/4}}{De^{1/2}})]\end{aligned} \tag{4.24}$$

Matching with the elastic Rayleigh solution on the '$-$' side gives:

$$B_{6L} = i\sqrt{2}kB_2 \tag{4.25}$$

$$\begin{aligned}&B_{4L} + B_{5L}\Big\{\frac{\sqrt{\pi/k}(-2)^{(-3/4)}(i-1)(-i)^{1/2}}{\sqrt{2}}\Big\} + B_{6L}\Big\{\frac{-i(1+3\log 2+2\log(ik))}{4\sqrt{2}k}\Big\}\\ &= -B_1^- - B_2[\log 2 - \log(\frac{E^{-1/4}}{De^{1/2}})]\end{aligned} \tag{4.26}$$

From the above expressions, one can see that the number of unknown constants are more than the number of equations, and hence all the constants cannot be determined via direct matching. We therefore neglect the constant terms B_{4L} and B_{4R}, and the resulting consistent system leads to the following dispersion relation:

$$\Big[\coth\left[k(1-y_c)\right]+\coth\left[ky_c\right]\Big]=\frac{1}{k\sqrt{2E}}\Big[1+7\log 2-i\pi+2\log\left(ik\right)-4\log\left(\frac{1}{E^{1/4}De^{1/2}}\right)\Big]\quad(4.27)$$

One can easily see that the above relation does not lead to sensible values of y_c in the elastic limit. Hence, in the limit De being finite but large, the two travelling-wave continuous spectra will no longer be preserved, and it will not be possible to find the resulting discrete spectra via a mere perturbation of the Case eigenfunctions (Case (1960)) in relaxation boundary layers around the travelling wave singularities. This is because the inner relaxation boundary layers, as seen above, do not support non-trivial solutions with the constraints that are imposed by the outer elastic boundary layer solutions on either side (for $\xi \to \pm\infty$).

The above statement reflects the fact that the functional forms of discrete eigenfunctions do not look anything like the Case eigenfunctions (Case (1960)). We might then to recognize the fact that the length scale of the discrete spectrum eigenfunction would adjust itself to being so small that relaxation terms become important at leading order everywhere in the domain. This would be via the viscous term because accounting for a weak relaxation immediately leads to a small viscosity ($\propto 1/De$). The above is much like the Orr-sommerfeld - Rayleigh relation where we do have the 'viscous solutions' of the Orr-sommerfeld equation that have a scale of $O(Re^{-1/2})$, leading to viscosity being important at leading order througout the domain, that have no Rayleigh analogs. It appears that to capture the oscillatory behaviour of the solution away from the critical level, we may need to adopt a WKB approach, where the small parameter needed would be the inverse square root of the Mach number ($Ma_e \propto De.Re$). Such an approach is actually adopted, for large Re, for a general non-linear flow, and this is illustrated in Drazin & Reid (1981). In this sense, the situation for elastic Couette flow is more akin to that of a non-linear flow in the absence of elasticity.

Chapter 5

Conclusions and Future Work

In this thesis, we studied the spectral characteristics of the elastic Rayleigh equation, the one that governs the evolution of small-amplitude perturbations in the limit $Re, De \rightarrow \infty$ with their ratio (E) being finite. Our focus was on the continuous spectra of this equation; in particular, as to how elasticity modifies the original inviscid continuous spectrum. For purposes of simplicity we restricted our study to two-dimensional petturtations for a pair of canonical shearing flows: plane Couette flow and the Rankine vortex. In the purely inviscid limit, both the Rankine vortex and plane Couette flow cases have virtually identical continuous spectra (notwithstanding the existence of a discrete mode in the vortex case). The continuous spectrum eigenfunctions for the radial and normal velocity fields, respectively, exhibit a kink corresponding to the presence of a vortex sheet at the critical level. With the addition of elasticity, we therefore expect the structure of the continuous spectrum modes to be modified in an analogous manner in both cases.

The detailed spectral analysis for elastic Couette flow was carried out in chapter [2]. Here, we examined analytically the effects of elasticity in the limit of small but finite E. Even for small E, elasticity plays an important role in the vicinity of the critical-level. The inertial terms become vanishingly small here due to the vanishing Doppler frequency; the elastic terms, however, remain finite since the base-state shear at the critical level remains finite. The neglect of the relaxation terms in the limit $De \rightarrow \infty$ implies that the polymer solution supports undamped elastic shear waves propagating relative to the base-state flow. As a result, the addition of elasticity leads to multiple (three) continuous spectra associated with the elastic Rayleigh equation. One of the spectra is associated with the critical-level that extends over the base-state range of velocities, the next being the fast shear-wave-spectrum (FSWS) that extends from $-\sqrt{2E}$ to $1-\sqrt{2E}$, and finally, the slow-shear-wave-spectrum (SSWS) that extends from $\sqrt{2E}$ to $1+\sqrt{2E}$. The underlying physics for the multiple continuous spectra, with the addition of elasticity, may thought of as being related to existence of three sub-patterns all of which can travel at the same velocity (the critical level velocity) - the first is a pattern that is convected by the flow at the critical level; the second and third are patterns that propagate, relative to the flow at locations separated from the critical level by $\sqrt{2E}$, at speeds of $\pm\sqrt{2E}$. In chapter [3], a similar analysis was carried out for the case of Rankine vortex, and the appropriate elastic generalization of the inviscid Kelvin mode is obtained. In both chapters [2] and [3], we investigate the problem in the framework of a matched asymptotic expansions approach, showing that the structure of the original inviscid eigenfunctions is modified in a boundary layer of thickness $O(\sqrt{E})$ around the critical level.

After studying the effects of elasticity in the limit $Re \to \infty$, $De \to \infty$, which is equivalent to neglecting the relaxation terms, in chapter [4], we retained the leading order relaxation contributions, by considering the limit where De is large but finite. An analytical approach involving a multiple-boundary layer analysis, with an inner relaxation layer, was carried out for each of the three singular points of the original elastic Rayleigh equation. Only the continuous spectrum associated with the critical level is found to survive for finite De; the pair of travelling-wave spectra is not preserved at finite De.

It was found in chapter [4] that the effect of relaxation on the singular travelling-wave eigenfunctions of the elastic Rayleigh equation will not be restricted to an asymptotically thin relaxation layer around the original critical point. This suggests future work along the lines of a WKB approach, for large but finite De, for the plane Couette flow studied in chapter [4]. It might be possible to extend this same analysis to the Rankine vortex. Effects of elasticity on inviscid dynamics (on the algebraic transient growth that occurs in the inviscid limit, for instance) can be studied by posing an elastic initial-value problem (IVP), and this may allow one to see the manner in which the singular elastic continuous spectrum modes superpose to reproduce an evolving initial condition. Also, since the limit considered above (Re, $De \to \infty$) allows one to draw an analogy of viscoelastic flows with magnetohydrodynamic flows in the limit of $Re_m \to \infty$ (Ogilvie & Proctor (2003)), Re_m being the magnetic Reynolds number, our findings may be of use in the astrophysical analog of the problem.

References

Azaiez, J. & Homsy, G.M. 1994 Linear stability of free shear flow of viscoelastic liquids. *J. Fluid Mech.* **268**, 37–69.

Balmforth, N.J. & Morrison, P.J. 1995*a* Normal modes and continuous spectra. *Annals of the New York Academy of Sciences* **773**, 80–94.

Balmforth, N.J. & Morrison, P.J. 1995*b* *Singular eigenfunctions for shearing fluids I.*. Institute for Fusion studies, University of Texas, Austin, Report No. 692.

Bird, R. B., Armstrong, R. C. & Hassager, O. 1987 *Dynamics of polymeric liquids. Volume 1 - Fluid Mechanics.*. John Wiley and Sons.

Boger 1977 A highly elastic constant-viscosity fluid. *J. Non-Newton. Fluid Mech.* **3(1)**, 87–91.

Case, K.M. 1960 Stability of inviscid plane couette flow. *Phys. Fluids* **3**, 143.

Coleman, B. D. & Noll, W. 1961 Foundations of linear viscoelasticity. *Rev. Mod. Phys.* **33**, 239–249.

Dabade, V., Navaneeth K.M. & Subramanian, G 2015 Effects of inertia and viscoelasticity on sedimenting anisotropic particles. *J. Fluid Mech.* .

Drazin, P, G & Reid, W, H 1981 *Hydrodynamic Stability*. Cambridge University Press.

Dyke, M. Van 1975 *Perturbation methods in fluid meachnics*. The Parabolic Press.

Engevik, L. 1971 A note on a stability problem in hydrodynamics. *Acta Mechanica* **12**, 143–153.

Fjortoft, R. 1950 *Geophys.* Oslo,17,1.

Frank W. J. Olver, Daniel W. Lozier, Ronald F. Boisvert Charles W. Clark 2010 *NIST Handbook of Mathematical Functions*. Cambridge Press.

Friedman, Bernard 1962 *Principles and Techniques of Applied Mathematics*. Springer.

Gorodtsov, V. & Leonov, A. 1967 On a linear instability of a plane parallel couette flow of viscoelastic fluids. *J. Appl. Math. Mech.* **31**, 289–299.

Graham, M. D. 1998 Effect of axial flow on viscoelastic taylor-couette instability. *J. Fluid Mech.* **360**, 341–374.

Groisman, A. & V.Steinberg 2000 Elastic turbulence in a polymer solution flow. *Nature* **405**, 53–55.

Howard, L.N. & Gupta, A.S. 1962 On the hydrodynamic and hydromagnetic stability of swirling flows. *J. Fluid Mech.* **14**, 463.

Joseph, D.D. 2007 *Fluid dynamics of viscoelastic liquids*. Springer.

Kaffel, A. & Renardy, M. 2010 On the stability of plane parallel viscoelastic shear flows in the limit of infinite weissenberg and reynolds numbers. *J. Non-Newtonian Fluid Mech.* .

Kumar, A. Sameer & Shankar, V. 2005 Instability of high-frequency modes in viscoelastic plane couette flow past a deformable wall at low and finite reynolds number. *J. Non-Newtonian Fluid Mech.* **125**, 121–141.

Kupferman, R. 2005 On the linear stability of plane couette flow for an oldroyd-b fluid and its numerical approximation. *J. Non-Newton. Fluid Mech.* **127**, 169–190.

Larson, R.G. 1988 *Constitutive equations for polymer melts and solutions*. Butterworths.

Larson, R.G., Shaqfeh, E.S.G. & Muller, S.J. 1990 A purely elastic instability in taylor-couette flow. *J. Fluid Mech.* **218**, 573–600.

Macosko, Christopher W. 1994 *Rheology principles, measurements, and applications*. WILEY-VCH.

M.E.McIntyre & Weissman, M.A. 1978 On radiating instabilities and resonant over reflection. *J. Atmospheric Sciences.* **35**, 1190–1196.

Miller, J.C. 2005 *Shear flow instabilities in viscoelastic fluids.*. PhD thesis, Cambridge University Press.

Ogilvie, G.I. & Proctor, M.R.E. 2003 On the relation between viscoelastic and magnetohydrodynamic flows and their instabilities. *J. Fluid Mech.* **476**, 389–409.

Porteous, K.C. & M.M.Denn 1972 Linear stability of plane poiseuille flow of viscoelastic liquids. *Transactions of the society of Rheology* **16:2**, 295–308.

Rallison, J.M. & Hinch, E.J. 1995 Instability of a high-speed submerged elastic jet. *J. Fluid Mech.* **288**, 311–324.

Rayleigh, Lord 1945 *Theory of Sound, Vol. II*. Dover.

Reddy, J.S.K., Roy, A. & Subramanian, G. 2015 Elastic instability of a vortex column. *J. Fluid Mech (manuscript under preparation).* .

Renardy, M. 1992 A rigorous stability proof for plane couette flow of an upper convected maxwell fluid at zero reynolds number. *Eur. J. Mech. B* **11**, 511–516.

Renardy, M. 2008 Stability of viscoelastic shear flows in the limit of high weissenberg and reynolds numbers. *J. Non-Newtonian Fluid Mech.* **155**, 124–129.

RENARDY, Y. & RENARDY, M. 1986 Linear stability of plane couette flow of an upper convected maxwell fluid. *J. Non-Newtonian Fluid Mech.* **22**, 23–33.

ROY, A. 2012 *Singular Eigenfunctions in Hydrodynamic Stability : The Roles of Rotation, Stratification and Elasticity*. PhD thesis, JNCASR.

ROY, A. & SUBRAMANIAN, G. 2014*a* Linearized oscillations of a vortex column: the singular eigenfunctions. *J.Fluid Mech.* **741**, 404–460.

ROY, A. & SUBRAMANIAN, G. 2014*b* Normal mode interpretation of the 'lift-up' effect. *J. Fluid Mech.* **757**, 82–113.

SAZONOV, I.A. 1989 Interaction of continuous spectrum waves with each other and discrete spectrum waves. *Fluid Dynamics Research* **4**, 586.

SLAVYANOV, S. YU & LAY, W 2000 *Special functions: a unified theory based on singularities*. Oxford Press.

TREFETHEN, L.N. 2000 *Spectral Methods in MATLAB*. SIAM.

VAN KAMPEN, G. 1955 On the theory of stationary waves in plasmas. *Physica* **51**, 949–963.

WILSON, H., RENARDY, M. & RENARDY, Y. 1999 Structure of the spectrum in zero reynolds number shear flow of the ucm and oldroyd-b liquids. *J. Non-Newton. Fluid Mech.* **80**, 251–268.